ELSEVIER

Biochimica et Biophysica Acta 1559 (2002) 96–120

BIOCHIMICA ET BIOPHYSICA ACTA
BBA

www.bba-direct.com

Conformational mapping of the N-terminal peptide of HIV-1 gp41 in membrane environments using ^{13}C-enhanced Fourier transform infrared spectroscopy

Larry M. Gordon [a,b,*], Patrick W. Mobley [c], Rosemarie Pilpa [c], Mark A. Sherman [d], Alan J. Waring [a,b,e]

[a] *Department of Pediatrics, Harbor-University of California at Los Angeles Medical Center, Research and Education Institute, Bldg. F5, 1124 West Carson Street, Torrance, CA 90502-2064, USA*
[b] *Department of Pediatrics, King-Drew Medical Center/UCLA, Los Angeles, CA, USA*
[c] *Chemistry Department, California State Polytechnic University, Pomona, CA, USA*
[d] *Physical Biochemistry Section, Division of Biology, Beckman City of Hope Medical Center, Duarte, CA, USA*
[e] *Department of Medicine, UCLA School of Medicine, Los Angeles, CA, USA*

Received 4 May 2001; received in revised form 11 October 2001; accepted 13 November 2001

Abstract

The N-terminal domain of HIV-1 glycoprotein 41 000 (FP; residues 1–23; AVGIGALFLGFLGAAGSTMGARSCO-NH_2) participates in fusion processes underlying virus–cell infection. Here, we use physical techniques to study the secondary conformation of synthetic FP in aqueous, structure-promoting, lipid and biomembrane environments. Circular dichroism and conventional, ^{12}C-Fourier transform infrared (FTIR) spectroscopy indicated the following α-helical levels for FP in 1-palmitoyl-2-oleoylphosphatidylglycerol (POPG) liposomes ~ hexafluoroisopropanol (HFIP) > trifluoroethanol (TFE) -> phosphate-buffered saline (PBS). ^{12}C-FTIR spectra also showed disordered FP structures in these environments, along with substantial β-structures for FP in TFE or PBS. In further experiments designed to map secondary conformations to specific residues, isotope-enhanced FTIR spectroscopy was performed using a suite of FP peptides labeled with ^{13}C-carbonyl at multiple sites. Combining these ^{13}C-enhanced FTIR results with molecular simulations indicated the following model for FP in HFIP: α-helix (residues 3–16) and random and β-structures (residues 1–2 and residues 17–23). Additional ^{13}C-FTIR analysis indicated a similar conformation for FP in POPG at low peptide loading, except that the α-helix extends over residues 1–16. At low peptide loading in either human erythrocyte ghosts or lipid extracts from ghosts, ^{13}C-FTIR spectroscopy showed α-helical conformations for the central core of FP (residues 5–15); on the other hand, at high peptide loading in ghosts or lipid extracts, the central core of FP assumed an antiparallel β-structure. FP at low loading in ghosts

Abbreviations: PBS, phosphate-buffered saline; HFIP, hexafluoroisopropanol; SDS, sodium dodecyl sulfate; TFE, trifluoroethanol; gp41, glycoprotein 41 000 of HIV-1; gp120, glycoprotein 120 000 of HIV-1; HA_2, influenza virus hemagglutinin protein; FP, HIV amino-terminal peptide 1–23 of gp41 (HIV-1 LAV_{1a} strain); SP-B_{1-25}, N-terminal peptide of human surfactant protein B (25 residues); RBC, red blood cells; LUV, large unilamellar vesicles; POPG, 1-palmitoyl-2-oleoylphosphatidylglycerol; POPC, 1-palmitoyl-2-oleoylphosphatidyl-choline; P/L, peptide to lipid molar ratio; C/P, cholesterol/phospholipid molar ratio; CD, circular dichroism; FTIR, Fourier transform infrared; ATR, attenuated total reflectance; TDC, transition dipole coupling; ESR, electron spin resonance; 2D-NMR, two-dimensional nuclear magnetic resonance; ESI, electrospray ionization; HIV-1, human immunodeficiency virus, type 1; HPLC, high performance liquid chromatography; CVFF, constant valence force field; PDB, Protein Data Bank

* Corresponding author, at address a. Fax: 310-222-6701. *E-mail address:* lgordon2@san.rr.com (L.M. Gordon).

PII: S0005-2736(01)00443-6

probably inserts deeply as an α-helix into the hydrophobic membrane bilayer, while at higher loading FP primarily associates with ghosts as an aqueous-accessible, β-sheet. In future studies, ^{13}C-FTIR spectroscopy may yield residue-specific conformations for other membrane-bound proteins or peptides, which have been difficult to analyze with more standard methodologies.

Keywords: Circular dichroism; Fourier transform infrared; Fusion; Isotope; Acquired immunodeficiency syndrome

1. Introduction

The amino-terminal peptide (FP; amino acids 1–23; Fig. 1) of glycoprotein 41 000 (gp41) has been proposed to be involved in the fusion activities underlying human immunodeficiency virus (HIV-1) infection of target cells [1]. In myxoviruses and paramyxoviruses, the fusion domain is a conserved hydrophobic amino acid sequence at the N-terminus of the viral envelope F_1 protein [2]. Gallaher [3] and Gonzalez-Scarano et al. [4] each observed extensive homologies of these sequences with those of the N-terminus of gp41, and suggested that the N-terminal gp41 peptide participates in the fusion of the HIV-1 envelope with host cells. When the HIV-1 glycoprotein 120 000 (gp120) binds to the lymphocyte CD4 receptor and one of several coreceptors of the chemokine family, the N-terminal gp41 domain is activated, which in turn may attack the target cell surface [2,5]. Recent physical studies [6–14] were interpreted as indicating that HIV-1 gp41 has a multimeric protein core that presents the N-terminal peptide as a trimer, similar to the low-pH-induced conformation of influenza virus hemagglutinin protein (HA_2) [15]. These findings suggest that gp41 shares aspects of the low-pH-induced 'spring-loaded' mechanism for HA_2, in which the N-terminal fusion peptide undergoes a major translocation [15,16]. According to one model, the N-terminus of HIV-1 gp41 inserts deeply into the host cell surface membrane [17], and the viral envelope gp41 couples the target cell surface to the HIV-1 lipid bilayer [18,19].

Experimental evidence has now accumulated confirming the participation of the N-terminal gp41 domain in HIV-1 mediated cytolytic and fusogenic processes. For example, site-directed mutagenesis studies indicated defective gp41 fusion activity for various modifications in the N-terminal domain, including substitutions of hydrophobic amino acids with polar residues [20–24], deletion of short amino acid sequences [25], or replacement of highly conserved Gly or Phe residues with Val [26,27]. A separate experimental approach has been to synthesize peptides based on the known N-terminal gp41 sequence, and then to determine whether the biological activity attributed to the peptide domain in the virus is also observed with the isolated peptide. For example, synthetic peptides based on the N-terminal domain of gp41 induced leakage of lipid vesicles [28–36], supporting the proposal that the N-terminus of gp41 is partly responsible for the cytolytic actions of whole HIV-1 virions. In agreement with this hypothesis is the finding that FP lysed both $CD4^+$ (cultured Hut-78 lymphocytes) and $CD4^-$ (human erythrocytes) cells [37,38]. Addition of N-terminal gp41 peptides to model liposomes also promoted lipid mixing [27–29, 31–34, 39–41]. With human erythrocytes, FP not only triggers rapid lipid mixing between cell membranes, but also induces multicell aggregates [38,42,43]. Of particular interest are the observations that selective modifications in synthetic N-terminal gp41 peptides reduced cytolytic and fusogenic activities, in parallel with the depressed syncytia-forming properties of the corresponding mutated full-length gp41 [27,33,35,39,40,42,43]. Furthermore, anti-HIV agents which block the membrane actions of the N-terminal gp41 peptide also reduce viral-mediated fusion [38,44–46]. Collectively, the above results suggest that critical fusogenic actions of HIV-1 gp41 are captured by synthetic N-terminal peptides.

Given the likely participation of the N-terminal gp41 region in HIV-1 fusion, it is important to elucidate the structure of this domain in membrane environments. The preferred approach would be to determine its three-dimensional structure using X-ray crystallography. However, previous X-ray analyses have been performed only on gp41 proteins lacking the N-terminal region, because full-length gp41 proteins do not form crystals [10–12,47]. Instead, circular dichroism (CD) and Fourier transform infrared

(FTIR) spectroscopy have been used to study the conformation of synthetic N-terminal gp41 peptides. These techniques indicated that N-terminal gp41 peptides assume variable proportions of α-helix, β-sheet, β-turn and random conformations when in structure-promoting solvents and membrane-mimics, depending on peptide length and concentration, solvent polarity, lipid charge and cation concentrations [17,28,29,31–35,39–41,43,48–53]. Furthermore, oriented FTIR spectra of the N-terminal gp41 peptide indicated an oblique insertion of the α-helix region into lipid bilayers [31,39]. Nevertheless, an important limitation of this earlier work is that CD and conventional FTIR spectroscopy are global methodologies that cannot assign conformations or orientations to individual amino acid residues within the peptide.

Accordingly, several 'residue-specific' techniques have been performed to define the conformation of N-terminal gp41 peptides in membrane-mimics. For example, CD spectra of FP and a series of truncated FP peptides in hexafluoroisopropanol (HFIP):H_2O (7:3, v/v) indicated an α-helical conformation for residues Ala-1 through Gly-13 [43]. Since amino acids that participate in defined secondary structure (i.e. α-helix or β-sheet) exchange amino hydrogens more slowly than residues in random structures, deuterium exchange followed by mass spectrometry was combined with CD spectroscopy to also map conformations to specific FP residues [51]. This joint analysis indicated that residues Gly-5 through Ala-15 were α-helical for FP in 70% HFIP, while only residues Leu-9 through Ala-15 were α-helical in the less structure-promoting solvent 50% trifluoroethanol (TFE) [51]. In a two-dimensional nuclear magnetic resonance (2D-NMR), CD and molecular modeling study of FP suspended in either TFE solvent or sodium dodecyl sulfate (SDS) detergent, Chang et al. [48,49] observed high levels of α-helix. Specifically, FP in 50% TFE assumed an α-helix conformation for residues Ile-4 to Ala-15, whereas the corresponding α-helix included residues Gly-5 to Gly-16 for FP bound to SDS micelles. With a 2D-NMR investigation of a FP analog in SDS, Vidal et al. [50] similarly reported that the hydrophobic core (~residues Gly-5 to Gly-16) folded in an α-helical conformation. However, caution must be employed in extrapolating these structural findings for N-terminal gp41 peptides in membrane-mimics to FP in membrane lipids. Experiments using truncated peptides to localize secondary structure such as Mobley et al. [43] introduce uncertainty, because shortened peptides may artificially fray at their unprotected N- and C-terminal ends. Moreover, the local FP conformations determined above in membrane-mimics (e.g. HFIP, TFE and SDS) may not faithfully reflect the corresponding structure in lipid bilayers.

Because of the inherent limitations of using mimics to simulate membrane environments, it is important to more directly assess the residue-specific conformation of FP in lipids and biological membranes using alternative experimental methodologies. In this article, we study the structure of the N-terminal HIV-1 gp41 peptide (FP) in phosphate-buffered saline (PBS), the membrane-mimic HFIP or TFE, or the lipid 1-palmitoyl-2-oleoylphosphatidylglycerol (POPG) using CD and conventional ^{12}C-FTIR spectroscopy. Additional FTIR experiments were conducted using a suite of ^{13}C-labeled FP to determine the residue-specific conformations of FP in the above membrane-mimic and lipid environments, and also erythrocyte ghosts and ghost lipid extracts. Earlier ^{13}C-FTIR spectroscopic investigations have indicated the versatility of this approach, demonstrating specific random, β-strand, β-turn and α-helical domains in soluble peptides [54,55], antiparallel β-sheet structures in amyloid peptides [56–58], α-helical coiled coils in model peptides [59], α-helix and orientation for discrete regions in the transmembrane domains of either phospholamban [60] or HIV-1 *vpu* [61], and α-helical regions in the transmembrane domain of influenza hemagglutinin [62]. Isotope-enhanced ^{13}C-FTIR spectroscopy has been previously combined with energy minimizations and molecular simulations to provide a comprehensive model of the N-terminal peptide of human surfactant protein B (SP-B_{1-25}) in POPG lipid, which specified locations for β-sheet, α-helix and random conformations [63]. Here we employ ^{13}C-FTIR techniques to examine in detail the polymorphic conformations that FP exhibits in membrane-mimic, model lipid bilayers, and human erythrocyte ghosts and ghost lipid extracts.

2. Materials and methods

2.1. Materials

Peptide synthesis reagents, included Fmoc amino acids and coupling solvents, were obtained from Applied Biosystems (Foster City, CA, USA). Deuterium was supplied by Aldrich (Milwaukee, WI, USA). Deuterated HFIP, TFE, and formic acid were obtained from Cambridge Isotope Laboratories (Andover, MA, USA). Fmoc ^{13}C-carbonyl alanine, glycine, leucine, and phenylalanine were purchased from Cambridge Isotope Laboratories. ^{13}C-Carbonyl phenylalanine was converted to the Fmoc derivative by AnaSpec (San Jose, CA, USA). POPG was obtained from Avanti Polar Lipids (Alabaster, AL, USA). R_{18}, octadecyl rhodamine B, was from Molecular Probes (Eugene, OR, USA). All organic solvents used for sample synthesis, purification and preparation were high performance liquid chromatography (HPLC) grade or better.

2.2. Solid-phase peptide synthesis, purification and characterizations

The 23-amino acid N-terminal sequence of gp41 (FP; Fig. 1) of the HIV-1 strain LAV_{1a} was prepared with either an ABI 431A peptide synthesizer or a

FP [Native N-terminal segment of HIV-1 gp41, residues 1-23]

NH_2 A V G I G A L F L G F L G A A G S T M G A R S $CONH_2$

$FP_{A1/G3}$ [FP, ^{13}C-carbonyl labeled at Ala-1, Gly-3]

NH_2 **A*** V **G*** I G A L F L G F L G A A G S T M G A R S $CONH_2$

$FP_{A1/G3/G5/L7}$ [FP, ^{13}C-carbonyl labeled at Ala-1, Gly-3, Gly-5, Leu-7]

NH_2 **A*** V **G*** I **G*** A **L*** F L G F L G A A G S T M G A R S $CONH_2$

$FP_{G5/A6}$ [FP, ^{13}C-carbonyl labeled at Gly-5, Ala-6]

NH_2 A V G I **G*** **A*** L F L G F L G A A G S T M G A R S $CONH_2$

$FP_{G5\text{-}A15}$ [FP, ^{13}C-carbonyl labeled at Gly-5 through Ala-15]

NH_2 A V G I **G*** **A*** **L*** **F*** **L*** **G*** **F*** **L*** **G*** **A*** **A*** G S T M G A R S $CONH_2$

$FP_{L7/L9/L12}$ [FP, ^{13}C-carbonyl labeled at Leu-7, Leu-9, Leu-12]

NH_2 A V G I G A **L*** F **L*** G F **L*** G A A G S T M G A R S $CONH_2$

$FP_{G13\text{-}G16}$ [FP, ^{13}C-carbonyl labeled at Gly-13 through Gly-16]

NH_2 A V G I G A L F L G F L **G*** **A*** **A*** **G*** S T M G A R S $CONH_2$

$FP_{G20/A21}$ [FP ^{13}C-carbonyl labeled at Gly-20, Ala-21]

NH_2 A V G I G A L F L G F L G A A G S T M **G*** **A*** R S $CONH_2$

Fig. 1. Amino acid sequences of the native N-terminal peptide (FP) of HIV-1 gp41, and seven FP variants labeled with ^{13}C at distinct positions. The N-terminal gp41 peptide is from the HIV-1 strain LAV_{1a} with the sequence 1–23, corresponding to residues 519–541 using the numbering of Myers et al. [64]. Amino acids are represented by one-letter codes, and those residues labeled with ^{13}C-carbonyls are indicated with bolded letters and asterisks.

Protein Technologies Symphony/Multiplex SPPS synthesizer, and purified by reverse phase HPLC as described earlier [45]; FP encompasses amino acid residues 519–541 of HIV-1 gp41 [64]. The following ^{13}C-carbonyl enhanced FP analogues were similarly prepared: $FP_{A1/G3}$, $FP_{A1/G3/G5/L7}$, $FP_{G5/A6}$, FP_{G5-A16}, $FP_{L7/L9/L12}$, $FP_{G13-G16}$ and $FP_{G20/A21}$ (Fig. 1). After HPLC purification, the peptides were twice freeze-dried from 0.01 M HCl to remove any residual acetate counterions that might interfere with FTIR measurements. The expected molecular masses of FP and isotope-enhanced FP analogues were obtained by fast-atom bombardment (FAB) and electrospray ionization (ESI) mass spectrometry (UCLA Center for Molecular and Medical Sciences Mass Spectrometry). Quantitative amino acid compositions for the peptides were determined at the UCLA Protein Microsequencing Facility.

2.3. Rationale for ^{13}C-site-directed FP substitutions

To probe the secondary conformations within FP, FTIR spectroscopy was conducted with site-directed, isotope-enhanced peptides. Specifically, ^{13}C-carbonyl groups were incorporated into multiple, neighboring amino acid residues of synthetic FP peptides (Fig. 1). Separate peptides were prepared with 'cassettes' of multiply ^{13}C-enhanced substitutions that were staggered to sequentially cover the peptide (Fig. 1). In earlier studies [54,55,60–63], cassettes of similarly ^{13}C-enhanced peptides permitted local domain mapping of various secondary conformations (e.g. α-helix, β-sheet, β-turn and random). The principal rationale behind these experiments is that the secondary structure with a peptide (or protein) usually extends over more than several adjacent residues [65].

2.4. Preparation of POPG liposomes for spectroscopic studies

Large unilamellar vesicles (LUV) of POPG in PBS (120 mM NaCl, 2.7 mM KCl, 10 mM Na_2HPO_4, pH 7.4) were prepared by extrusion through polycarbonate filters [66]. A dry lipid film was hydrated with buffer-saline solution, followed by vortexing of the dispersion to form multilamellar vesicles. The suspension was freeze thawed five times, and then extruded through 100 nm pore size polycarbonate filters (Nuclepore, Pleasanton, CA, USA) fives times using a LipoFast device (Avestin, Ottawa, ON, Canada). The size distribution of extruded unilamellar vesicles was determined by dynamic light scattering with a Microtrac 9230 UPA ultrafine particle analyzer (Leeds and Northrup, St. Petersburg, FL, USA) [67]. Extrusion through the 100 nm pore filters yielded a single population of POPG vesicles with a mean diameter of 95.8 nm and a standard deviation of 20.3 nm. LUV were suspended at 500 nmoles lipid/ml PBS buffer for spectroscopic studies.

2.5. Preparation of human erythrocyte ghosts and lipid extracts from erythrocyte ghosts

Ghosts were isolated from human erythrocytes, obtained from outdated units from the local Blood Bank [68] and suspended in the isotonic PBS buffer. Lipids were extracted by incubating ghosts with isopropanol [69]. The lipid extract was concentrated by low-temperature, low-pressure rotary evaporation. Lipid phosphorus was quantified as described earlier [17].

2.6. CD spectroscopy

CD measurements were made with an AVIV 62DS spectropolarimeter (AVIV Associates, Lakewood, NJ, USA), fitted with a thermoelectric controller that maintained the same temperature at 25°C [63,70,71]. Peptide solutions or peptide:liposome suspensions were measured in 0.1 mm light path demountable cells scanned from 250 to 185 nm at a rate of 10 nm/min and a sample interval of 0.2 nm. The instrument was routinely calibrated with (+)-10-camphorsulfonic acid (1 mg/ml) and a 1 mm path length cell [72], and the ellipticity expressed as the mean residue ellipticity, $[\Theta]_{MRE}$ (deg cm^2 dmol^{-1}). Peptide sample concentrations were determined from quantitative amino acid analysis (UCLA Microsequencing Facility).

The α-helical structure of FP peptides in solvent or lipid environments was determined from CD spectra with the following methodology. The percentage of α-helical conformation in the peptide was estimated using the formalism of Chen et al. [73]. This approach assumes the maximum theoretical ellipticity

for a given peptide or protein at 222 nm may be derived from the number of amino acid residues (n), and the ellipticity at 222 nm of a helix of infinite length described by Eq. 1:

$$\%\ \alpha - \text{helix} = [\Theta]_{MRE}/[-39500(1-(2.57/n))]\text{deg cm}^2\ \text{dmol}^{-1} \quad (1)$$

2.7. FTIR spectroscopy

Infrared spectra were recorded at 25°C using either a Mattson Series FTIR spectrometer (Drew University) or Bruker Vector 22 FTIR spectrometers (California State Polytechnic University, Pomona and Harbor-UCLA REI) equipped with DTGS detectors, averaged over 256 scans at a gain of 4 and a resolution of 2 cm^{-1} [43,63,70]. For FTIR spectra of FP originally in solvents, peptide self-films were prepared by air drying peptide solutions in 100% HFIP onto 50×20×2 mm 45° attenuated total reflectance (ATR) crystals fitted for either the Bruker (Pike Technologies, Madison, WI, USA) or Mattson (Spectral Solutions, Canyon, CA, USA) spectrometers. The dried peptide self-films were then overlaid with solution containing deuterated solvents (i.e. deuterated HFIP:water:formic acid (70:30:0.1, v/v), TFE:water:formic acid (50:50:0.1, v/v) or PBS (pH 7.4)) prior to spectral acquisition; control deuterated solvent samples were similarly prepared, but without peptide. Spectra of FP peptides in solvent were obtained by subtraction of the deuterated solvent spectrum from the peptide-deuterated solvent spectrum. For measurements with peptides in a lipid environment, FP peptides were added to LUV of POPG from 100% HFIP, and incubated with the liposomes for 1 h. FTIR spectra were recorded on the above unchromatographed peptide:liposome mixtures, and also on these peptide:lipid samples after passing through a Sephadex G-50 column to remove non-liposome-associated peptide [31]. Chromatographed and unchromatographed lipid–peptide samples were dried onto the ATR crystal. POPG lipid–peptide samples, and also control POPG lipid samples without peptide, were hydrated for 2 h with nitrogen-D_2O vapor, before spectral measurement. The FP in POPG lipid spectrum was obtained by subtracting the POPG lipid with D_2O hydration spectrum from that of FP in POPG with D_2O hydration. Peptide/lipid (P/L) ratios were determined here using the earlier finding of Martin et al. [31] that the peptide concentration is proportional to the area (S_{amide}) of the amide I band (1680–1600 cm^{-1}), while the lipid concentration is proportional to the area ($S_{\nu(C=O)lipid}$) of the lipid ν(C=O) band (1770–1700 cm^{-1}). Therefore, the peptide/lipid ratio is proportional to the following ratio: $(S_{amide})/(S_{\nu(C=O)lipid})$.

FTIR spectroscopy was also performed on FP peptides added to either human red blood cell ghosts, or lipids extracted from ghosts. Using a concentrated peptide–HFIP stock solution, FP was added to ghosts suspended in 5 mM phosphate buffer (pH 7.0) to yield the indicated P/L ratio and a final HFIP concentration of 3%; control ghosts were similarly prepared but omitting peptide. FTIR spectra of peptide in ghosts at 25°C were obtained by subtraction of the control ghost spectrum from the corresponding spectrum of peptide in ghosts with 3% HFIP. For measurements on FP in erythrocyte lipids, peptide–lipid films were prepared by air drying an HFIP solution containing both peptides and red blood cell (RBC) ghost lipids onto the ATR crystal to form multilayers. The lipid–peptide sample was then hydrated for 2 h by passing D_2O vapor through ports in the ATR attachment cover plate. Control lipid samples were similarly prepared, but omitting peptide. FTIR spectra of peptide in ghost lipids at 25°C were obtained by subtraction of the ghost lipid spectrum from the corresponding spectrum of peptide in ghost lipids.

The amide I bands of conventional ^{12}C-FTIR spectra of FP self-films and chromatographed lipid:peptide samples were analyzed for the various secondary conformations [63,70]. For determinations with peptide:liposomes, the spectrum of the lipid film without peptide (i.e. band centered at 1730 cm^{-1}) was subtracted from that of samples with peptide associated with lipid. The proportions of α-helix, β-turn, β-sheet and disordered conformations were determined by Fourier self-deconvolutions for band narrowing and area calculations of component peaks determined with curve-fitting software supplied by Mattson and based on methods described by Kauppine et al. [74]. The frequency limits for the different structures were as follows: α-helix, 1662–1645 cm^{-1}, β-sheet, 1637–1613 and 1710–1682 cm^{-1}, β-turns,

1682–1662 cm^{-1}, and disordered or random, 1650–1637 cm^{-1} [75–77].

Enhancement of FP peptides with site-specific ^{13}C-carbonyl groups permits the direct determination of those amino acid residues participating in secondary conformations. Since the stretching frequencies of the peptide backbone carbonyl groups are sensitive to local conformations, replacement of ^{12}C with ^{13}C should reduce the stretching frequency of an *isolated* carbonyl oscillator by $\sim$37 cm^{-1} [54,78–80]. In the absence of significant transition dipole coupling (TDC) interactions [81–83], the α-helix band should be lowered to 1625–1608 cm^{-1}, β-turns to 1645–1625 cm^{-1} and disordered or random to 1613–1600 cm^{-1}. These spectral shifts were detected by measuring FTIR spectra of the natural abundance and ^{13}C-enhanced peptides in various environments, and noting the positions of any new peaks in the ^{13}C-FTIR spectrum [54,60,63]. Subtle spectral shifts were also detected with difference FTIR spectra, obtained by subtracting the natural abundance spectrum from that of the isotopically enhanced peptide [54,63]. The difference FTIR spectra should show a negative peak at the original position of the conformational band, and a positive peak shifted from the original by $\sim$37 cm^{-1}. All spectra were presented here using Harvard ChartXL 3.0 (Serif; http://www.harvard-graphics.com).

2.8. Molecular modeling

The amino-terminal peptide (FP) of HIV-1 gp41 was modeled with Insight/Discover 97.0 software (Molecular Simulations, San Diego, CA, USA) running on a Silicon Graphics Indigo-2R10000 High Impact workstation (Beckman Research Institute City of Hope core facility). Energy minimizations and molecular dynamics were conducted using constant valence force field (CVFF) [84,85] within the Discover software environment. Ramachandran plots were determined for the FP structures derived from simulated annealing. The final refined model geometry parameters were evaluated by PROCHECK [86].

2.9. Coordinates

The coordinates for the 17 lowest energy structures of FP in the HFIP solution (i.e. HFIP:H_2O:HCOOH (70:30:01, v/v)), together with a full list of restraints, have been deposited in the Protein Data Bank (PDB) under the accession code 1ERF.

3. Results

3.1. CD spectroscopy of FP suspended in PBS, membrane-mimic and lipid environments

To determine the overall conformation of the N-terminal sequence of HIV-1 gp41 (FP) in a variety of environments, CD spectra were measured for peptide in an aqueous buffer, two membrane-mimic solvents, or a liposome suspension. CD spectra were recorded for FP suspended in two membrane mimetic solvents (i.e. TFE/H_2O/HCOOH (50:50:0.1, v/v) or HFIP/H_2O/HCOOH (70:30:0.1, v/v)) (not shown). The TFE and HFIP curves each demonstrate a characteristic double minimum at 208 and 222 nm with nearly equal negative peaks, suggesting substantial α-helical content for FP in these environments [51]. The alternative interpretation that these peaks reflect 3_{10} helix seems less likely, as recent CD spectra with model peptides that fold as 3_{10} helix [87] demonstrate an unusually intense 208 nm band relative to the 222 nm band. The corresponding spectrum (not shown) of FP with POPG liposomes in PBS, pH 7.4, after chromatography to remove unbound peptide, similarly indicates a broad double minimum at 208 and 222 nm that is characteristic of high α-helix. On the other hand, control CD spectra with FP alone in PBS, pH 7.4, exhibited low signal and high noise (not shown); these spectra suggested a lack of α-helix and considerable random structure for the peptide, in agreement with previous investigations [28,88].

It is worthwhile to quantitate the secondary conformations of FP with further analysis of the CD spectra. The percentage of α-helix conformation for this peptide was estimated from Eq. 1, as described in Section 2 [73]. This analysis demonstrated the following α-helical levels for FP in various environments: POPG $\sim$ HFIP > TFE > PBS (Table 1). The proportion of α-helix for FP in POPG (Table 1) indicates that $\sim$13 residues participate in α-helix for peptide incorporated into liposomes. The finding of

similar α-helical contents for FP in either POPG or HFIP (Table 1) suggests that the HFIP solvent accurately mimics the peptide environment of POPG liposomes. It should also be noted that the α-helical content for FP decreases in inverse proportion to the increasing water content, in the respective HFIP, TFE and PBS solvents. The relatively high noise and low signal for the CD spectrum of FP in PBS (not shown) is attributed to the formation of insoluble peptide aggregates. Previous electron spin resonance (ESR) studies of spin-labeled FP [45] indicated low solubility and elevated aggregation for peptide in PBS. Moreover, electron microscopy showed that the N-terminal gp41 peptide 519–540 formed filamentous, aggregated structures in aqueous medium [30].

Table 1
Proportions of secondary structure[a] for FP in solvents and POPG lipid dispersions, as estimated from Fourier self-deconvolution of the FTIR spectra of the peptide amide I band and CD spectra

System	% Conformation			
	α-Helix	β-Sheet	β-Turn	Disordered
FTIR spectra[b]				
HFIP[c]	52.0	11.5	22.5	14.1
TFE[d]	36.8	15.1	26.0	22.1
PBS[e]	19.6	32.3	23.0	25.1
POPG[f]	52.1	6.5	24.9	16.7
CD spectra[g]				
HFIP[h]	54.3	N.D.	N.D.	N.D.
TFE[i]	35.3	N.D.	N.D.	N.D.
PBS[j]	13.0	N.D.	N.D.	N.D.
POPG[k]	58.1	N.D.	N.D.	N.D.

[a]Data are the means of four separate determinations and have an S.E. ±5% or better.
[b]FTIR spectra were deconvoluted as described in Section 2 (Fig. 3).
[c]FP (470 μM) dried onto an ATR plate from 100% HFIP, and resolvated with deuterated HFIP/water/formic acid (70:30:0.1, v/v) (Fig. 2B).
[d]FP (470 μM) dried onto an ATR plate from 100% HFIP, and resolvated with deuterated TFE/water/formic acid (50:50:0.1, v/v) (Fig. 2C).
[e]FP (470 μM) dried onto an ATR plate from 100% HFIP, and resolvated with deuterated PBS, pH 7.4 (Fig. 2A).
[f]FP incorporated into POPG at an initial P/L ratio of 1/70 for LUV liposomes suspended in PBS, pH 7.4. Peptide/liposomes were chromatographed to remove non-lipid-associated FP, then dried onto the ATR plate, and resolvated with D_2O (Fig. 2D).
[g]CD spectra were analyzed using Eq. 1 of Section 2.
[h]FP (47 μM) in HFIP/water/formic acid (70:30:0.1, v/v).
[i]FP (47 μM) in TFE/water/formic acid (50:50:0.1, v/v).
[j]FP (10 μM) suspended in PBS, pH 7.4.
[k]FP incorporated into POPG at an initial P/L ratio of 1/70 for LUV liposomes suspended in PBS, pH 7.4. Peptide/liposomes were chromatographed to remove non-lipid-associated FP.

3.2. Conventional ^{12}C-FTIR spectroscopy of FP in PBS, membrane-mimic and lipid environments

The secondary conformations of FP in the above solvent and lipid systems were next studied using conventional ^{12}C-FTIR spectroscopy. Representative FTIR spectra of the amide I band for FP in the PBS, HFIP, TFE and POPG systems are shown in Fig. 2. A principal band occurs at 1657 cm^{-1} for the HFIP (Fig. 2B), TFE (Fig. 2C) and POPG (Fig. 2D) spectra, consistent with high α-helical content for FP in these membrane-mimic and lipid environments [89]. Extensive prior FTIR studies of deuterated proteins [75,76,90,91] have assigned bands in the range 1650–1659 cm^{-1} as α-helical. Small low- and high-field shoulders at 1628 and 1696 cm^{-1} also indicate significant amounts of an antiparallel β-sheet component for FP in the TFE solvent (Fig. 2C). Contrarily, the FTIR spectrum of FP in the PBS medium (Fig. 2A) exhibited a dominant peak at 1628 cm^{-1}, a high-field shoulder of 1643 cm^{-1} and a minor high-field peak at 1696 cm^{-1}. The major peak at 1628 cm^{-1} and minor peak at 1696 cm^{-1} in Fig. 2A indicate extensive antiparallel β-sheet for FP in PBS, created by strong interstrand and, to a lesser degree, intrastrand TDC interactions [81–83]; the high-field shoulder at approx. 1643 cm^{-1} also denotes significant random structure for FP in PBS. Similar FTIR spectra were observed for a range of aqueous amyloid peptides, and were also attributed to high proportions of antiparallel β-sheet structures [56–58].

The relative proportions of secondary structure were determined with subsequent curve fitting of the above FTIR spectra, using the criteria of Byler and Susi [75]. A typical Fourier self-deconvolution and curve-fitting analysis is shown for FP in the TFE solvent (Fig. 3). In agreement with the above CD findings (Table 1), Fig. 3 indicates that the predominant component is an α-helix (centered at 1657 cm^{-1}) for FP in TFE (Table 1). This analysis also showed significant β-sheet (1628 and 1696 cm^{-1} bands), β-turn (1670 cm^{-1} band) and random (1643

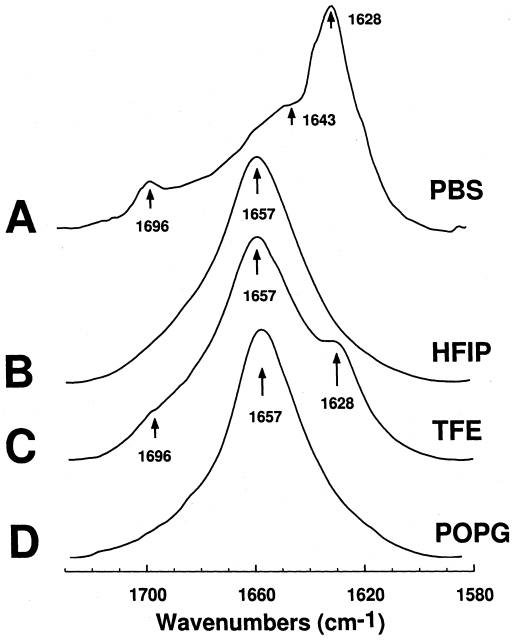

Fig. 2. FTIR spectra of the amide I band of FP in PBS, HFIP and TFE solutions and POPG liposomes at 25°C, with experimental conditions in Section 2. (A) FP concentration was 470 μM in deuterated PBS, pH 7.4. The arrows at 1628 and 1696 cm^{-1} denote a β-sheet component, while the shoulder at 1643 cm^{-1} also indicates random structure. (B) FP concentration was 470 μM in deuterated HFIP/water/formic acid (70:30:0.1, v/v). (C) FP concentration was 470 μM in deuterated TFE/water/formic acid (50:50:0.1, v/v). (D) FP was added to POPG liposomes at an initial P/L of 1/70, suspended in PBS, pH 7.4. Peptide:liposomes were chromatographed to remove non-lipid-associated peptide, as described in Section 2. Spectra were recorded on chromatographed peptide:liposomes that were dried on the ATR and hydrated with D_2O for 2 h. The arrows at 1657 cm^{-1} in B–D indicate a dominant α-helix component for FP in these membrane-mimic environments; there is a pronounced shoulder peak at 1628 cm^{-1} and a minor peak at 1696 cm^{-1} in C that also indicates β-sheet structure for FP in TFE solution. Spectra have been normalized for comparison. The abscissa for each spectrum (left to right) is 1730–1580 cm^{-1}, while the ordinate represents absorption (in arbitrary units).

cm^{-1} band) structures for FP in TFE (Fig. 3; Table 1). Summing each of these components yielded a predicted FP in TFE spectrum that agreed well with the corresponding experimental spectrum (Fig. 3). Consistent with the CD results, additional Fourier self-deconvolutions of the FTIR spectra confirmed the following α-helical levels for FP in the various environments: POPG ~ HFIP > TFE > PBS (Table 1). These results are of interest, since CD spectroscopy uses continuously solvated samples, while ATR-FTIR spectroscopy subjects samples to a drying and resolvation step. Our comparable findings with the two spectroscopic techniques argue against the drying and resolvation step introducing significant experimental artifacts into the FTIR spectral analysis. In parallel with the respective decreases in α-helix conformation observed for FP in the TFE or PBS environments, increases were noted in β- and random structures (Table 1). These findings suggest that moving FP from a lipid (or membrane-mimic) milieu to a more aqueous environment transforms certain α-helical residues into β- or random conformations. Indeed, Table 1 demonstrates that β-sheet, β-turn and random conformations assume greater than 80% of the total secondary structure for FP in PBS, while the corresponding α-helical content is less than 20%.

The association of FP with POPG liposomes was quantified by recording ^{12}C-FTIR spectra, before (not shown) and after chromatographing peptide:lipid mixtures. For POPG incubated with FP at an initial calculated P/L ratio of 1/70, the $(S_{amide})/(S_{\nu(C=O)lipid})$ ratio for unchromatographed and chromatographed samples indicated >90% peptide uptake by liposomes. These results are consistent with the relatively low solubility of the peptide in PBS

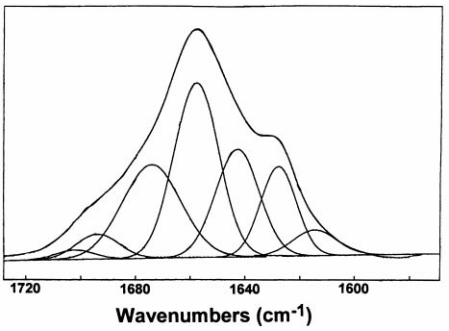

Fig. 3. Representative FTIR spectrum and curve fitting of the amide I band of native FP in the TFE solution. Top curve is the experimental FTIR spectrum of the amide I band, recorded at 25°C (see Fig. 2C). Frequency limits for different secondary structures were as follows: α-helix, 1662–1645 cm^{-1}; β-sheet, 1637–1613 cm^{-1} and 1710–1682 cm^{-1}; β-turn, 1682–1662 cm^{-1}; and disordered (random) structure, 1650–1637 cm^{-1}. The % contributions for each component are shown in Table 1. Overlapping the experimental spectrum is the predicted spectrum, obtained by summing the above components. The peptide concentration was 470 μM, suspended in TFE/water/formic acid (50:50:0.1, v/v).

buffer, and a strong association between the amphipathic FP and the POPG liposomes [28].

3.3. Isotopically enhanced ^{13}C-FTIR spectroscopy of FP in membrane-mimic and lipid environments

Although the above ^{12}C-FTIR spectroscopic findings indicate that FP assumes distinct conformations in the HFIP, TFE, PBS and POPG systems (Figs. 2 and 3; Table 1), it is not possible using only these data to assign secondary structure (e.g. α-helix, β-turn, β-sheet, random) to particular residues. To probe for local conformations, isotopically enhanced, FTIR spectroscopy was performed with FP labeled with ^{13}C-carbonyls at multiple sites, staggered to sequentially cover the peptide (Fig. 1).

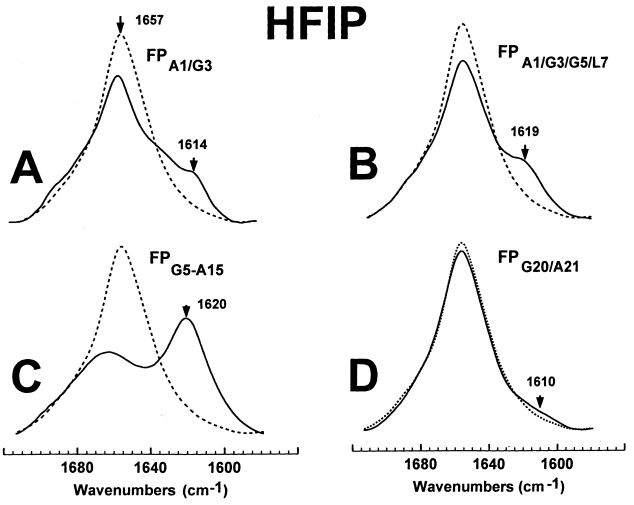

Fig. 4. FTIR spectra of the amide I band for the ^{12}C-carbonyl (i.e. 'native') FP peptide and a suite of multiply ^{13}C-carbonyl-enhanced FP peptides in HFIP solution (see Fig. 1 for amino acid sequences). Peptides were suspended at 470 μM concentration in deuterated HFIP:water:formic acid (70:30:0.1, v/v). Spectra were recorded at 25°C on peptide which was first dried on the ATR from 100% HFIP solution, and then resolvated with deuterated HFIP:water:formic acid (70:30:0.1, v/v) (see Section 2). (A) $FP_{A1/G3}$ is the solid line and native FP is the dashed line. The amide I band is shown for the native FP spectrum, with a dominant α-helical component centered at 1657 cm^{-1}. The minor peak at 1614 cm^{-1} in the $FP_{A1/G3}$ spectrum indicates α-helical character with some disorder for Ala-1 and Gly-3. (B) $FP_{A1/G3/G5/L7}$ (solid line), FP (dashed line). The minor peak at 1619 cm^{-1} in the $FP_{A1/G3/G5/L7}$ spectrum indicates α-helical components for Ala-1, Gly-3, Gly-5 and Leu-7. (C) FP_{G5-A15} (solid line), FP (dashed line). The major peak at 1620 cm^{-1} in the FP_{G5-A15} spectrum indicates a strong α-helical component for Gly-5, Ala-6, Leu-7, Phe-8, Leu-9, Gly-10, Phe-11, Leu-12, Gly-13, Ala-14 and Ala-15. (D) $FP_{G20/A21}$ (solid line), FP (dashed line). The minor peak at 1610 cm^{-1} in the $FP_{G20/A21}$ spectrum indicates random (disordered) structure for Gly-20 and Ala-21. The abscissa for each spectrum (left to right) is 1720–1560 cm^{-1}, while the ordinate represents absorption (in arbitrary units).

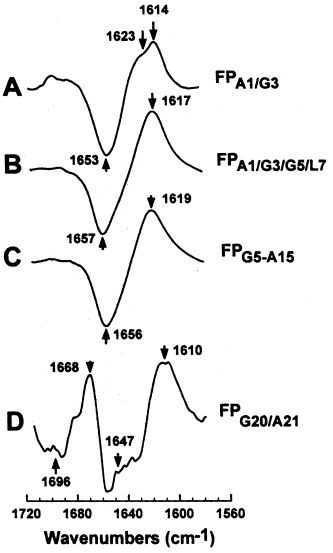

Fig. 5. Difference FTIR spectra of FP peptides in HFIP solution, obtained by subtracting the spectrum of the native ^{12}C-carbonyl FP from those of ^{13}C-enhanced FP peptides. (A) FP spectrum (dashed line in Fig. 4A) from $FP_{A1/G3}$ (solid line in Fig. 4A). The negative peak at 1653 cm^{-1} (arrow), and the positive peak at 1614 cm^{-1} and high-field shoulder at 1623 cm^{-1} (arrows) indicate a mix of α-helix and random conformations for Ala-1 and Gly-3. (B) FP spectrum (dashed line in Fig. 4B) from $FP_{A1/G3/G5/L7}$ (solid line in Fig. 4B). The negative peak at 1657 cm^{-1} and the positive peak at 1617 cm^{-1} (arrows) indicate α-helix conformations for Ala-1, Gly-3, Gly-5 and Leu-7. (C) FP spectrum (dashed line in Fig. 4C) from FP_{G5-A15} (solid line in Fig. 4C). The negative peak at 1656 cm^{-1} and the positive peak at 1619 cm^{-1} (arrows) indicate α-helix conformations for Gly-5, Ala-6, Leu-7, Phe-8, Leu-9, Gly-10, Phe-11, Leu-12, Gly-13, Ala-14 and Ala-15. (D) FP spectrum (dashed line in Fig. 4D) from $FP_{G20/A21}$ (solid line in Fig. 4D). The negative peak at 1647 cm^{-1} and the positive peak at 1610 cm^{-1} (arrows) indicate random conformations, while the negative peak at 1702 cm^{-1} and the positive peak at 1668 cm^{-1} denote β-sheet conformations, for Gly-20 and Ala-21. See Fig. 1 for amino acid sequences of the native and ^{13}C-enhanced FP peptides. The abscissa for each spectrum (left to right) is 1720–1560 cm^{-1}, while the ordinate represents Δ(absorption), in arbitrary units. The peak-to-trough amplitudes for each spectrum were normalized.

For peptides in the strongly helix-promoting HFIP environment (Fig. 2B; Table 1), Fig. 4 shows the natural abundance, ^{12}C-FTIR spectrum of FP and the isotopically enhanced ^{13}C-FTIR spectra of FP

labeled with ^{13}C-carbonyls at Ala-1 and Gly-3 ($FP_{A1/G3}$), Ala-1, Gly-3, Gly-5 and Leu-7 ($FP_{A1/G3/G5/L7}$), Gly-5 to Ala-15 (FP_{G5-A15}), or Gly-20 and Ala-21 ($FP_{G20/A21}$). There are major differences between the native and cassette FP spectra, which are attributed to the presence of ^{13}C-carbonyl groups. In the $FP_{A1/G3/G5/L7}$ spectrum (Fig. 4B), there is a decrease in the area 1662–1645 cm^{-1} corresponding to an α-helical component, and a concurrent increase in the area 1625–1608 cm^{-1}, indicating an isotopic shift of ~37 cm^{-1}. The nature of this isotopic shift may also be visualized in a difference FTIR spectrum, obtained by subtracting the native FTIR spectrum (dashed line in Fig. 4B) from that of the $FP_{A1/G3/G5/L7}$ spectrum (solid line in Fig. 4B); the resulting difference FTIR spectrum (Fig. 5B) confirms the presence of negative and positive bands centered at 1657 and 1617 cm^{-1}, respectively. The simplest interpretation of these results is that the isotope-induced shift of ~37 cm^{-1} in Figs. 4B and 5B is due to residues Ala-1, Gly-3, Gly-5 and Leu-7 participating in α-helix (Fig. 6), a peptide conformation in which intrastrand TDC interactions will probably be negligible [56,81–83].

The conformational center of FP in the HFIP solvent was similarly examined by comparing the native FTIR spectrum with that of a FP analogue with ^{13}C-carbonyls at Gly-5 to Ala-15 (FP_{G5-A15}). The FTIR spectra in Fig. 4C and the difference FTIR spectrum in Fig. 5C indicate both substantial decreases in the area 1662–1645 cm^{-1} and correspondingly large increases in the area 1625–1608 cm^{-1}, consistent with an isotopic shift of ~37 cm^{-1}. The predominant peak at 1620 cm^{-1} in the FP_{G5-A15} spectrum (Fig. 4C) argues that a high proportion of amino acid residues between Gly-5 and Ala-15 probably assumes an α-helical conformation (Fig. 6). To further test this assignment, FTIR spectra were recorded for FP and FP_{G5-A15} incorporated into SDS micelles suspended in PBS at a P/L of 1/70 (not shown). Earlier residue-specific 2D-NMR and molecular modeling investigations on FP in SDS micelles (P/L of 1/

System	^{13}C-Peptides	1 NH$_2$-Ala	2 Val	3 Gly	4 Ile	5 Gly	6 Ala	7 Leu	8 Phe	9 Leu	10 Gly	11 Phe	12 Leu	13 Gly	14 Ala	15 Ala	16 Gly	17 Ser	18 Thr	19 Met	20 Gly	21 Ala	22 Arg	23 Ser -CONH$_2$
		Peptide Conformation																						
HFIP	$FP_{A1/G3/G5/L7}$	α		α		α		α																
	$FP_{A1/G3}$	R/α		R/α																				
	$FP_{G5/A6}$					(<---α--->)																		
	FP_{G5-A15}					(<---------- α-helix----------->)																		
	$FP_{L7/L9/L12}$							α		α			α											
	$FP_{G13-G16}$													(<------- βT------->)										
	$FP_{G20/A21}$																				(<-R/β ->)			
TFE	$FP_{A1/G3/G5/L7}$	βT/R		βT/R		βT/R		βT/R																
	$FP_{A1/G3}$	βT/R		βT/R																				
	$FP_{G5/A6}$					(<- β ->)																		
	FP_{G5-A15}					(<---------- α-helix/β-sheet/R----------->)																		
	$FP_{L7/L9/L12}$							α/β		α/β			α/β											
	$FP_{G13-G16}$													(<------- R ------>)										
	$FP_{G20/A21}$																				(<-βT/R->)			
POPG	$FP_{A1/G3/G5/L7}$	α		α		α		α																
	$FP_{A1/G3}$	α		α																				
	$FP_{G5/A6}$					(<- α ->)																		
	FP_{G5-A15}					(<---------- α-helix----------->)																		
	$FP_{L7/L9/L12}$							α		α			α											
	$FP_{G13-G16}$													(<------- βT------->)										
	$FP_{G20/A21}$																				(<-R/β ->)			

Fig. 6. Conformational map of the N-terminal peptide (FP) of HIV-1 gp41 in HFIP, TFE and POPG liposome environments, as estimated from the FTIR spectra of ^{13}C-labeled peptides. Amino acids are represented by three-letter codes. Codes (in parentheses) for peptide conformations are: β-sheet (β), β-turn (βT), α-helix (α) and random (R). For FP (470 μM) in HFIP:water:formic acid (70:30:0.1, v/v), secondary conformations were determined from the FTIR spectra of Figs. 4, 5 and 9. For FP (470 μM) in TFE:water:formic acid (50:50:0.1, v/v), secondary conformations were determined from the FTIR spectra of Figs. 7 and 9. For FP with POPG in PBS (pH 7.4) at an initial peptide/lipid ratio of 1/70, secondary conformations were determined from the FTIR spectra of Figs. 8 and 10.

150) demonstrated α-helix for residues Gly-5 to Gly-16 [49]. In the present studies, ^{12}C-FTIR spectra of FP in SDS indicated a major peak at 1658 cm^{-1}, while ^{13}C-FTIR spectra of $FP_{G5–A15}$ in SDS showed a decrease in the peak centered at 1658 cm^{-1} and a new peak at 1621 cm^{-1} (not shown), consistent with α-helical structure for residues Gly-5 to Ala-15. Our FTIR spectral findings agree with the prior determination of Chang et al. [49] that the center of FP in SDS assumes an α-helical conformation. Furthermore, the similarities between the spectra of FP and $FP_{G5–A15}$ in SDS (not shown) with the corresponding spectra of these peptides in HFIP (Fig. 4C) confirm that, for FP in HFIP solution, residues Gly-5 to Ala-15 are also α-helical.

Control experiments were performed to assess whether intermolecular TDC interactions between ^{13}C-carbonyls contributed to the peak in the HFIP $FP_{G5–A15}$ spectrum at 1620 cm^{-1} (Fig. 4C) [81–83]. The ^{13}C-labeled $FP_{G5–A15}$ was diluted with unlabeled FP (i.e. 1 part ^{13}C-peptide:1 part ^{12}C-peptide and 1 part ^{13}C-peptide:3 parts ^{12}C-peptide). FTIR spectra of these 'isotopically diluted' peptide mixtures in the HFIP solvent indicated a reduced ^{13}C-signal at 1620 cm^{-1}, but no frequency shift (not shown). These FTIR results are consistent with the 1620 cm^{-1} peak in Fig. 4C representing a localized amide I absorption due to α-helix.

Secondary conformations at the N- and C-terminal regions of FP in the HFIP solvent were also analyzed using FP analogues with ^{13}C-carbonyls at Ala-1 and Gly-3 ($FP_{A1/G3}$) or Gly-20 and Ala-21 ($FP_{G20/A21}$). Fig. 4D shows a small decrease in the $FP_{G20/A21}$ spectrum in the area 1658–1640 cm^{-1} with respect to the native FP spectrum, along with a concomitant increase in the area 1625–1595 cm^{-1}, suggestive of a random conformation for residues Gly-20 and Ala-21. In agreement with this assignment, the resulting difference FTIR spectrum in Fig. 5D demonstrates a negative band centered at ~1647 cm^{-1} and a positive band at 1610 cm^{-1}, consistent with an isotopic shift of ~37 cm^{-1} for random conformations. Interestingly, the difference FTIR spectrum in Fig. 5D further shows a smaller negative band centered at ~1698 cm^{-1} and a correspondingly small positive band at ~1668 cm^{-1}, indicative of Gly-20 and Ala-21 simultaneously assuming limited β-sheet conformation (Fig. 6). Multiple conformations were similarly identified for Ala-1 and Gly-3 at the extreme N-terminus of FP. Fig. 4A shows a decrease in the $FP_{A1/G3}$ spectrum in the area 1665–1640 cm^{-1}, as well as an enhanced broad band centered at ~1614 cm^{-1}. Furthermore, the corresponding difference FTIR spectrum (Fig. 5A) demonstrates a large negative band centered at 1653 cm^{-1}, with a principal positive band at 1614 cm^{-1} and a high-field shoulder at 1623 cm^{-1}. The simplest interpretation for the heterogeneous $FP_{A1/G3}$ spectra (Figs. 4A and 5A) is that the N-terminal Ala-1 and Gly-3 residues assume polymorphic conformations, exhibiting both random and α-helical character (Fig. 6). The finding of multiple conformations for the carbonyl groups at the N-terminal end of the α-helix for FP suggests some fraying of the helix for residues Ala-1 to Gly-3. Our inability to detect any random structures in the $FP_{A1/G3/G5/L7}$ spectra (Figs. 4B and 5B) is probably due to the high α-helical content in residues Gly-5 and Leu-7 masking the relatively low proportion of random conformation in residues Ala-1 and Gly-3 (see below).

For peptides in the TFE solvent that produced lower α-helix and more β-structure than the HFIP environment (Figs. 2C and 3; Table 1), an analogous ^{13}C-FTIR analysis was performed to localize these secondary conformations within FP. Fig. 7B demonstrates a decrease in the region 1685–1645 cm^{-1} for the $FP_{A1/G3/G5/L7}$ spectrum, with new peaks centered at 1643 and 1608 cm^{-1}, respectively. The 1643 cm^{-1} peak in the $FP_{A1/G3/G5/L7}$ spectrum (Fig. 7B) represents a shift of ~37 cm^{-1} from the native band between 1682 and 1662 cm^{-1} (Fig. 3), indicating that Ala-1, Gly-3, Gly-5 and Leu-7 adopt a β-turn conformation in the TFE environment (Fig. 6). The additional peak in Fig. 7B centered at 1608 cm^{-1} shows a shift of ~37 cm^{-1} from the native band between 1650 and 1637 cm^{-1} (Fig. 3), indicating that Ala-1, Gly-3, Gly-5 and Leu-7 assume random conformations in addition to the β-turn structures (Fig. 6). FTIR spectra of $FP_{A1/G3/G5/L7}$ 'isotopically diluted' with native ^{12}C-FP confirmed the absence of intermolecular TDC contributions to the new ^{13}C-peaks at 1643 (β-turn) and 1608 cm^{-1} (random) peaks (not shown). Multiple conformations were also observed in the center of FP, for peptides suspended in the TFE solvent. Fig. 7C shows a marked decrease in the region 1680–1640 cm^{-1} for the

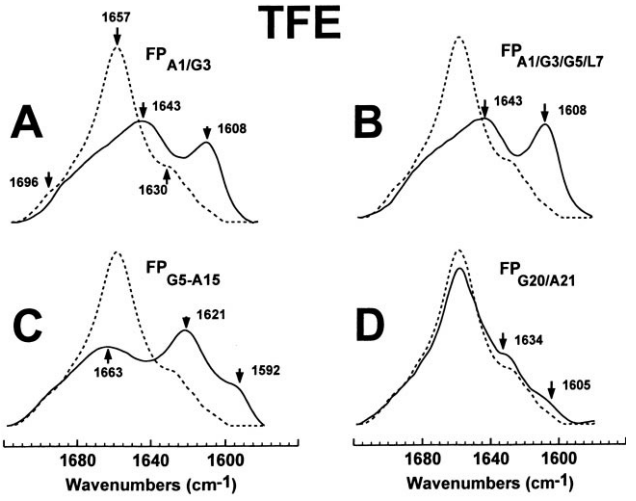

Fig. 7. FTIR spectra of the amide I band for the ^{12}C-carbonyl (i.e. 'native') FP peptide and a suite of multiply ^{13}C-carbonyl-enhanced FP peptides in TFE solution. Peptides were suspended at 470 μM concentration in deuterated TFE:water:formic acid (50:50:0.1, v/v). Spectra were recorded at 25°C on peptide which was first dried on the ATR from 100% HFIP solution, and then resolvated with deuterated TFE:water:formic acid (50:50:0.1, v/v) (see Section 2). (A) $FP_{A1/G3}$ is the solid line and native FP is the dashed line. The amide I band is shown for the native FP spectrum, with a dominant α-helical component centered at 1657 cm^{-1} and a minor peak at 1630 cm^{-1} denoting β-sheet. The $FP_{A1/G3}$ spectrum indicates broad peaks at 1643 and 1608 cm^{-1}, denoting both β-turn and random structure for Ala-1 and Gly-3. (B) $FP_{A1/G3/G5/L7}$ (solid line), FP (dashed line). The peaks at 1643 and 1608 cm^{-1} in the $FP_{A1/G3/G5/L7}$ spectrum indicate β-turn and random components for Ala-1, Gly-3, Gly-5 and Leu-7. (C) FP_{G5-A15} (solid line), FP (dashed line). The major and minor peaks at 1621 and 1593 cm^{-1}, respectively, in the FP_{G5-A15} spectrum indicate strong α-helical and minor β-sheet components for Gly-5, Ala-6, Leu-7, Phe-8, Leu-9, Gly-10, Phe-11, Leu-12, Gly-13, Ala-14 and Ala-15. (D) $FP_{G20/A21}$ (solid line), FP (dashed line). The minor peaks at 1634 and 1605 cm^{-1} in the FP_{G20A21} spectrum indicate β-turn and random (disordered) structures for Gly-20 and Ala-21. The abscissa for each spectrum (left to right) is 1720–1560 cm^{-1}, while the ordinate represents absorption (in arbitrary units).

FP_{G5-A15} spectrum, with a new peak at 1621 cm^{-1} and a low-field shoulder at 1592 cm^{-1}. The 1621 cm^{-1} peak in the FP_{G5-A15} spectrum (Fig. 7C) denotes a shift of ~37 cm^{-1} from the native band between 1662 and 1645 cm^{-1} (Fig. 3), indicating that Gly-5 through Ala-15 assume α-helix conformations in TFE (Fig. 6). The low-field shoulder in Fig. 7C at 1592 cm^{-1} is due to a shift of ~37 cm^{-1} from the native band at 1637–1613 cm^{-1} (Fig. 3), indicating that Gly-5 through Ala-15 adopt minor β-sheet in addition to α-helical conformations (Fig. 6). The similarity between the FTIR spectra of $FP_{A1/G3}$ (Fig. 7A) and $FP_{A1/G3/G5/L7}$ (Fig. 7B), with pronounced peaks at 1643 and 1608 cm^{-1}, confirms that Ala-1 and Gly-3 simultaneously assume β-turn and random structures in the TFE solvent (Fig. 6). The new minor peaks centered at 1634 and 1605 cm^{-1} for the FTIR spectrum of $FP_{G20/A21}$ in TFE (Fig. 7D) also indicate β-turn and random conformations for Gly-20 and Ala-21 (Fig. 6).

It is important to also consider whether ^{13}C-FTIR

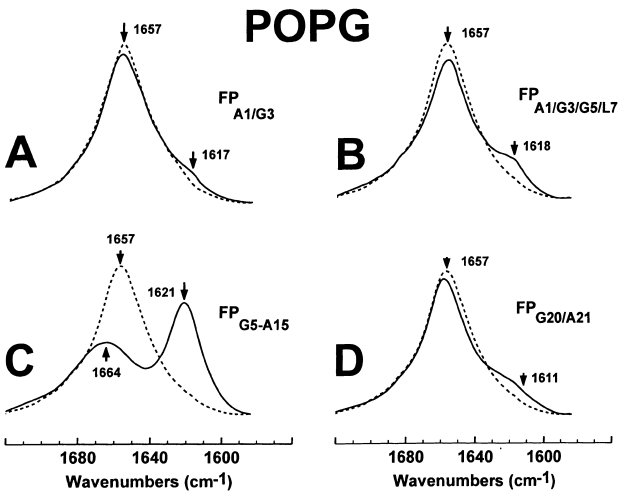

Fig. 8. FTIR spectra of the amide I band for the ^{12}C-carbonyl (i.e. 'native') FP peptide and a suite of multiply ^{13}C-carbonyl-enhanced FP peptides in POPG liposomes. Peptides were suspended in POPG liposomes at an initial P/L ratio of 1/70, and chromatographed to remove unincorporated peptides as described in Section 2. Spectra were recorded on chromatographed peptide:liposomes that were dried on the ATR and hydrated with D_2O for 2 h. (A) $FP_{A1/G3}$ is the solid line and native FP is the dashed line. The amide I band is shown for the native FP spectrum, with a dominant α-helical component centered at 1657 cm^{-1}. The minor peak at 1617 cm^{-1} in the $FP_{A1/G3}$ spectrum indicates α-helical character. (B) $FP_{A1/G3/G5/L7}$ (solid line), FP (dashed line). The minor peak at 1618 cm^{-1} in the $FP_{A1/G3/G5/L7}$ spectrum indicates α-helical components for Ala-1, Gly-3, Gly-5 and Leu-7. (C) FP_{G5-A15} (solid line), FP (dashed line). The major peak at 1620 cm^{-1} in the FP_{G5-A15} spectrum indicates a strong α-helical component for Gly-5, Ala-6, Leu-7, Phe-8, Leu-9, Gly-10, Phe-11, Leu-12, Gly-13, Ala-14 and Ala-15. (D) $FP_{G20/A21}$ (solid line), FP (dashed line). The minor peak at 1611 cm^{-1} in the $FP_{G20/A21}$ spectrum indicates random (disordered) structure for Gly-20 and Ala-21. The abscissa for each spectrum (left to right) is 1720–1560 cm^{-1}, while the ordinate represents absorption (in arbitrary units).

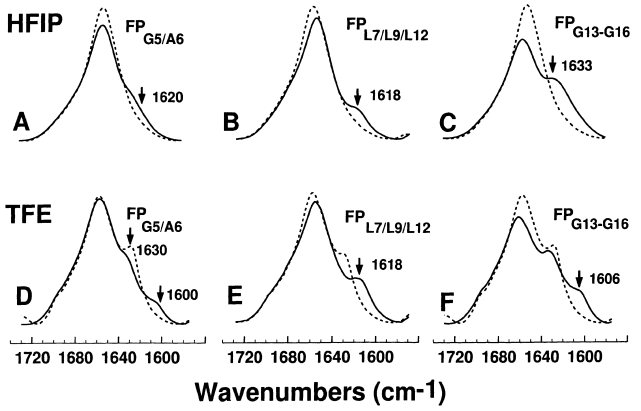

Fig. 9. FTIR spectra of the amide I band for the ^{12}C-carbonyl (i.e. 'native') FP and a suite of FP labeled with multiple ^{13}C-carbonyls in the central region, for peptides in the HFIP or TFE solution. Peptides were suspended at 470 μM in deuterated HFIP:water:formic acid (70:30:0.1, v/v) (A–C) or TFE:water:formic acid (50:50:0.1, v/v) (D–F); spectra were recorded at 25°C on peptide dried from 100% HFIP and resolvated on the ATR from the respective deuterated solutions (see Section 2). (A) $FP_{G5/A6}$ (solid line), FP (dashed line). The minor peak at 1620 cm^{-1} in the $FP_{G5/A6}$ spectrum indicates α-helical components for Gly-5 and Ala-6, for peptide in the HFIP solvent. (B) $FP_{L7/L9/L12}$ (solid line), FP (dashed line). The minor peak at 1618 cm^{-1} indicates α-helical components for Leu-7, Leu-9 and Leu-12 in the HFIP solvent. (C) $FP_{G13–G16}$ (solid line), FP (dashed line). The shoulder at 1633 cm^{-1} represents β-turn elements for residues Gly-13, Ala-14, Ala-15 and Gly-16 in the HFIP solvent. (D) $FP_{G5/A6}$ (solid line), FP (dashed line). The minor peak at 1600 cm^{-1} in the $FP_{G5/A6}$ spectrum indicates a β-sheet component for Gly-5 and Ala-6, for peptide in the TFE solvent. (E) $FP_{L7/L9/L12}$ (solid line), FP (dashed line). The minor peak at 1618 cm^{-1} indicates α-helical components for Leu-7, Leu-9 and Leu-12 in the TFE solvent. (F) $FP_{G13–G16}$ (solid line), FP (dashed line). The minor peak at 1606 cm^{-1} represents random structure for residues Gly-13, Ala-14, Ala-15 and Gly-16 in the TFE solvent. The abscissa for each spectrum (left to right) is 1740–1560 cm^{-1}, while the ordinate represents absorption (in arbitrary units).

spectral analysis may similarly be used to map the local conformations of FP in an actual lipid bilayer environment. Fig. 8B shows a decrease in the region 1670–1645 cm^{-1} for the $FP_{A1/G3/G5/L7}$ spectrum with a new peak centered at 1618 cm^{-1}, indicating that Ala-1, Gly-3, Gly-5 and Leu-7 are α-helical in POPG (Fig. 6). A more marked decrease occurs in the region 1670–1640 cm^{-1} for the $FP_{G5–A15}$ spectrum with a pronounced new peak centered at 1621 cm^{-1} (Fig. 8C), indicating that Gly-5 through Ala-15 assume α-helix conformations in POPG (Fig. 6). Residues Ala-1 and Gly-3 at the N-terminus of FP in POPG are also assigned as α-helix (Fig. 6), since the ^{13}C-FTIR spectrum of $FP_{A1/G3}$ (Fig. 8A) is depressed in the region 1650–1660 cm^{-1} over the native FTIR spectrum, with a new peak at 1617 cm^{-1}. ^{13}C-FTIR spectroscopy also indicated that the C-terminus of FP in POPG liposomes exhibited random conformations. The new peak at 1611 cm^{-1}, along with a depressed 1660–1640 cm^{-1}, for the $FP_{G20/A21}$ spectrum (Fig. 8D) indicates that Gly-20 and Ala-21 assume random or disordered conformations in POPG liposomes (Fig. 6). Of particular interest are the similarities in the FTIR spectra of 'cassette' ^{13}C-labeled peptides in either the HFIP solvent (Fig. 4) or POPG liposomes (Fig. 8), indicating that FP in the HFIP environment accurately mimics the behavior of this peptide when incorporated into lipid bilayers (Fig. 6).

The conformational fine structure within the central core of FP in the HFIP, TFE, and POPG environments was further probed using fusion peptides labeled with ^{13}C-carbonyls at Gly-5 and Ala-6 ($FP_{G5/A6}$), Leu-7, Leu-9 and Leu-12 ($FP_{L7/L9/L12}$) and Gly-13, Ala-14, Ala-15 and Gly-16 ($FP_{G13–G16}$)

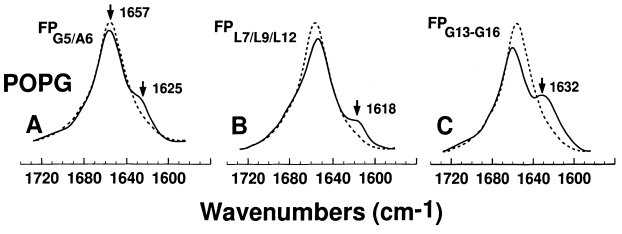

Fig. 10. FTIR spectra of the amide I band for the ^{12}C-carbonyl (i.e. 'native') FP and a suite of FP labeled with multiple ^{12}C-carbonyls in the central region, for peptides in POPG liposomes. Peptides were suspended in POPG liposomes at an initial P/L ratio of 1/70, and chromatographed to remove unincorporated peptides as described in Section 2. Spectra were recorded on chromatographed peptide:liposomes that were dried on the ATR and hydrated with D_2O for 2 h. (A) $FP_{G5/A6}$ (solid line), FP (dashed line). The minor peak at 1625 cm^{-1} in the $FP_{G5/A6}$ spectrum indicates α-helical components for Gly-5 and Ala-6, for peptide in POPG liposomes. (B) $FP_{L7/L9/L12}$ (solid line), FP (dashed line). The minor peak at 1618 cm^{-1} indicates α-helical components for Leu-7, Leu-9 and Leu-12 in POPG liposomes. (C) $FP_{G13–G16}$ (solid line), FP (dashed line). The shoulder at 1632 cm^{-1} represents β-turn elements for residues Gly-13, Ala-14, Ala-15 and Gly-16 in POPG liposomes. The abscissa for each spectrum (left to right) is 1740–1560 cm^{-1}, while the ordinate represents absorption (in arbitrary units).

(Figs. 9 and 10). For peptides in the HFIP solvent, the new peaks at 1620 and 1618 cm^{-1} for the $FP_{G5/A6}$ and $FP_{L7/L9/L12}$ spectra (Fig. 9A,B), respectively, confirm that Gly-5, Ala-6, Leu-7, Leu-9 and Leu-12 assume α-helical conformations (Fig. 6). On the other hand, the $FP_{G13-G16}$ spectrum (Fig. 9C) for peptide in HFIP solvent indicates a new band at 1633 cm^{-1}, indicating that Gly-13, Ala-14, Ala-15 and Gly-16 adopt a β-turn conformation (Fig. 6); these findings suggest that this GAAG sequence represents the C-terminal cap of the α-helix (see below). Interestingly, the spectra of $FP_{G5/A6}$, $FP_{L7/L9/L12}$ or $FP_{G13-G16}$ (Fig. 10A–C) in POPG liposomes are very similar to the corresponding ^{13}C-FTIR spectra of these analogues in the HFIP solvent (Fig. 9A–C), verifying again that the conformation of FP in the HFIP environment accurately mimics the structure of this peptide in lipids. Specifically, the new peaks at 1625 and 1618 cm^{-1} for the $FP_{G5/A6}$ and $FP_{L7/L9/L12}$ spectra (Fig. 10A,B), respectively, confirm that Gly-5, Ala-6, Leu-7, Leu-9 and Leu-12 are α-helical in POPG liposomes (Fig. 6). On the other hand, the $FP_{G13-G16}$ spectrum (Fig. 10C) for peptide in HFIP solvent indicates a new band at 1632 cm^{-1}, indicating that Gly-13, Ala-14, Ala-15 and Gly-16 assume a β-turn conformation in POPG (Fig. 6). For peptides in the TFE solvent, the FP core demonstrates significantly less α-helical structure (Fig. 9D–F). Although a new peak at 1618 cm^{-1} in the spectrum of $FP_{L7/L9/L12}$ in TFE indicates α-helical structure for Leu-7, Leu-9 and Leu-12 (Fig. 9E), the loss of the low-field shoulder at 1630 cm^{-1} and the extended tail to 1590 cm^{-1} argues that these residues concurrently exhibit β-sheet conformations (Fig. 6). Furthermore, the $FP_{G5/A6}$ in TFE spectrum (Fig. 9D) exhibits a loss of the 1630 cm^{-1} shoulder and a new peak at 1600 cm^{-1}, suggesting that Gly-5 and Ala-6 adopt a β-sheet structure (Fig. 6). Last, the $FP_{G13-G16}$ in TFE spectrum (Fig. 9F) shows a new peak at 1606 cm^{-1}, indicating random conformations for Gly-13, Ala-14, Ala-15 and Gly-16 (Fig. 6).

3.4. Molecular modeling of FP in HFIP and POPG lipid environments

Although the above ^{13}C-FTIR spectroscopic analysis assigned the conformation of the majority (i.e. 70%) of the amino acids for FP in the HFIP solvent, the conformations of a number of residues (i.e. Val-2, Ile-4, Ser-17, Thr-18, Met-19, Arg-22, Ser-23) were not experimentally determined. Molecular modeling was conducted to provide structural information on these 'gap' residues, and also to evaluate the conformational flexibility of domains within FP. From the ^{13}C-FTIR spectral results in Figs. 4 and 10, the initial structure was modeled as an α-helix, except for the terminal regions (residues 1–2 and 17–23) which were modeled as β-strands using Discover software. Twenty cycles of simulated annealing were performed, using a protocol published earlier [92], to examine those conformations accessible to the terminal regions and helix side chains. Throughout the simulation, constraints were applied to maintain not only the helix motif, but also the chirality of the amino acids in the L form. Using a time step of 0.5 fs, the system was equilibrated for 1000 iterations at 300 K. The temperature was then raised to 900 K in increments of 30 K over a period of 20 ps. Molecular dynamics was then carried out at 900 K for 30 ps, followed by annealing to a temperature of 300 K over 50 ps. The resulting structure was then energy minimized using 5000 steps of steepest descents, followed by 10 000 steps of conjugate gradients until the maximum derivative was less than 0.001. Throughout the simulation the backbone atoms of residues 3–16 (helix) were constrained using a force constant that increased by 25 (kcal/mol × $Å^2$) during each heating step. A similar torsional constraint was applied to all peptide bonds in order to maintain them in the *trans* conformation. During the final minimization, all constraints were removed.

With the residue-specific constraints based on ^{13}C-FTIR measurements described above, 17 molecular models representing possible conformations of FP in the HFIP solvent were generated by simulated annealing molecular dynamics. The superimposed conformers are shown as stick figures in Fig. 11A, whereas a ribbon representation of a selected conformer showing the location of each residue is indicated in Fig. 11B. The geometry parameters of the final models were evaluated using PROCHECK [86]. The Ramachandran plot in Fig. 12 confirms that the backbone torsion angles for all 17 conformers principally fall within the allowed regions. Moreover, the Ramachandran plot shows high levels of backbone

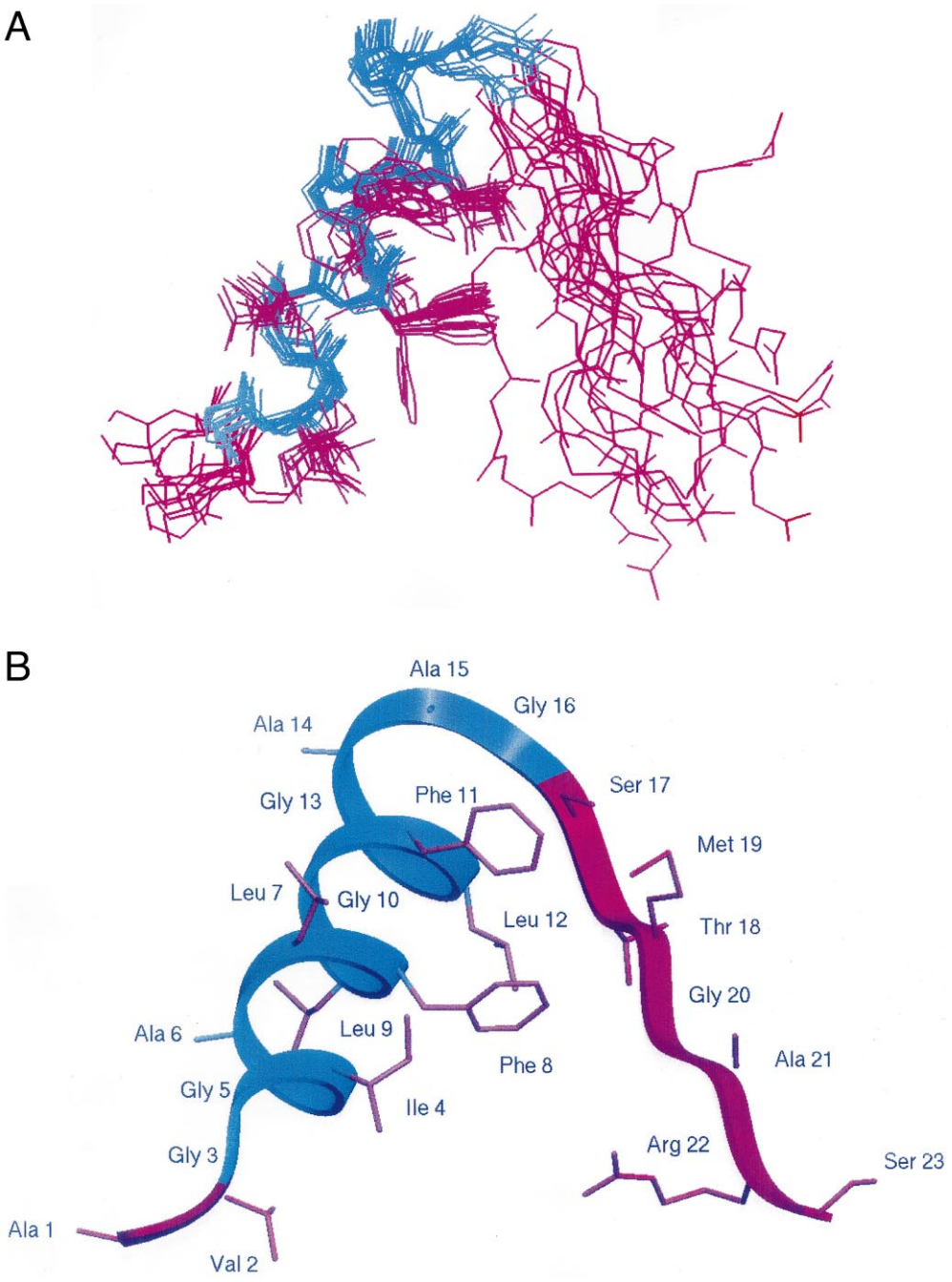

Fig. 11. Conformation dynamic model (A) and ribbon representation (B) of the N-terminal peptide (FP) of HIV-1 gp41 in HFIP solution. (A) Superimposed view of 17 solution structures of FP, calculating from simulated annealing, molecular dynamics and geometry optimization experiments. Constraints were imposed incorporating residue-specific information derived from FTIR spectroscopy of ^{13}C-labeled FP peptides in HFIP:water:formic acid (70:30:0.1, v/v). Conformer backbones in blue and purple indicate α-helical and extended β-strands, respectively; side chains are denoted by purple. (B) Ribbon representation of a selected conformer showing the location of each residue, with the same orientation as in A. Residues 3–16 encompass the α-helix (backbone shown in blue with side chains in purple), while residues 1–2 and 17–23 are extended β-sheet (backbone and side chains shown in purple).

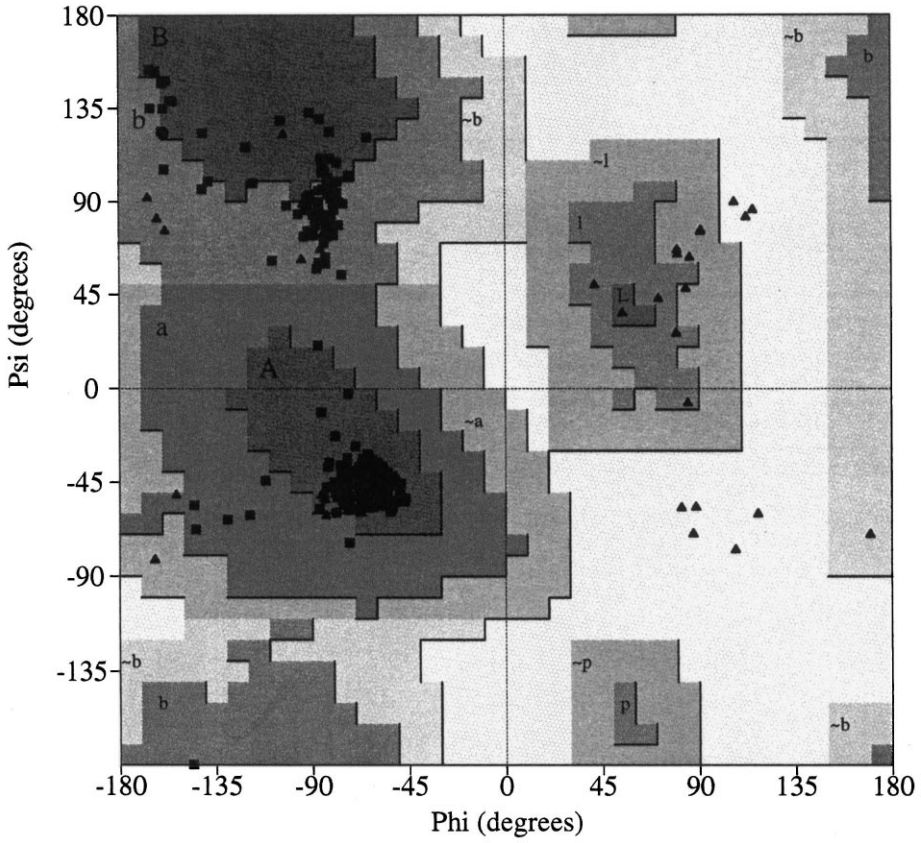

Fig. 12. Ramachandran plot [86] for the 17 best structures of the N-terminal peptide (FP) of HIV-1 gp41, derived from the simulated annealing experiments. Psi (torsional angle for the C_a–C bond axis) is plotted versus phi (torsional angle for the C_a–N bond axis). Initial constraints were obtained from residue-specific structural information derived from FTIR spectroscopy of ^{13}C-enhanced FP peptides in HFIP:water:formic acid (70:30:0.1, v/v). The dark areas represent most favored regions (A, B, L), while the light gray areas (a, b, l, p) and lightest gray areas (∼a, ∼b, ∼l, ∼p) represent additional allowed regions. Triangles denote glycine residues.

torsion angles lying in the α-helix and β-structural zones, consistent with the FP structure in the HFIP solvent primarily subdivided into α-helix and β-conformations (Fig. 6; Table 1). The superimposed conformers (Fig. 11A) capture the major structural features indicated by our ^{12}C- and ^{13}C-FTIR spectroscopic studies, namely an α-helix (residues 3–16) and extended β- and random structures (residues 1–2 and 17–23) with a high degree of flexibility. The fraying of the helix for residues 1–2 is consistent with the intrinsic instability of α-helices at the N-terminus, in which only the carbonyl groups for the first four helical residues participate in the hydrogen-bonding network. The capping pattern at the C-terminus of the α-helix (Fig. 11B) apparently involves residues Gly-13, Ala-14, Ala-15 and Gly-16.

The above molecular model developed for FP in the HFIP solvent may also be applied to the structure of FP in POPG liposomes, with some modifications. As may be seen from ^{13}C-FTIR spectroscopy of FP in POPG (Fig. 6), the α-helix extends from Ala-1 to Gly-16. Using these constraints, energy minimizations and molecular simulations indicated a model for FP in POPG that was nearly identical to that for FP in HFIP (Fig. 11A,B), except that residues Ala-1 and Val-2 also participate in the α-helix (not shown). Similar to that found for FP in HFIP, the molecular model for lipid FP exhibits a carboxyl terminus for the helix, with an α-helix cap consisting of Gly-13, Ala-14, Ala-15 and Gly-16 (not shown).

3.5. *Conventional ^{12}C- and isotopically enhanced ^{13}C-FTIR spectroscopy of FP in human erythrocyte ghosts and lipid extracts from ghosts*

An important remaining question focuses on

whether the structures determined here for HIV-1 FP in either membrane-mimics or POPG lipids (Figs. 6 and 11A,B) bear any relevance to the conformation of FP in biological membranes. Although previous studies have shown that FP induces lysis, aggregation and lipid mixing of POPG liposome vesicles [28,32], it may be argued that these negatively charged lipid vesicles are not a good model for the biomembranes (e.g. $CD4^+$ lymphocyte plasma membranes) targeted by HIV-1. Consequently, the above residue-specific structures determined for FP in POPG liposomes may not accurately represent FP conformations in key membranes involved in host-viral infections.

To address the above questions, further conventional ^{12}C-FTIR and ^{13}C-enhanced FTIR spectroscopy was conducted here on FP peptides added to both human erythrocyte ghosts and lipid extracts from ghosts. Human red blood cell ghosts should provide a more relevant experimental model than POPG liposomes, because the red cell bilayer lipid composition, asymmetry and molar cholesterol/phospholipid (C/P) ratio approximate those in both the target cells and the HIV-1 envelope [18]. Also it should be noted that addition of synthetic FP to intact red blood cells induces hemolysis, lipid mixing and aggregation [37,38,42,43,45,88]. At a low P/L ratio of 1/70, conventional ^{12}C-FTIR spectra of FP added to human erythrocyte ghosts showed a principal band occurring at 1655 cm^{-1} (Fig. 13A), consistent with high α-helical content for FP. A decrease occurs in the region 1663–1647 cm^{-1} for the ^{13}C-FTIR spectrum of FP_{G5-A15} with a new peak centered at 1620 cm^{-1} (Fig. 13A), confirming that residues Gly-5 through Ala-15 assume α-helix conformations in ghost membranes at low peptide loading. On the other hand, the ^{12}C-FTIR spectrum of FP with erythrocyte ghosts at a high P/L ratio of 1/10 (Fig. 13B) exhibited a dominant peak at 1627 cm^{-1}, and a small high-field peak at 1687 cm^{-1}, indicative of antiparallel β-sheet. Interestingly, the ^{12}C-FTIR spectrum in Fig. 13B of high FP-loaded ghosts bears striking similarities with that of FP in PBS (Fig. 2A), suggesting similar aqueous-accessible environments for the peptide. A decrease in absorption occurs in the region 1639–1612 cm^{-1} for the ^{13}C-FTIR spectrum of FP_{G5-A15} with a dominant new peak centered at 1587 cm^{-1} (Fig. 13B), consistent with

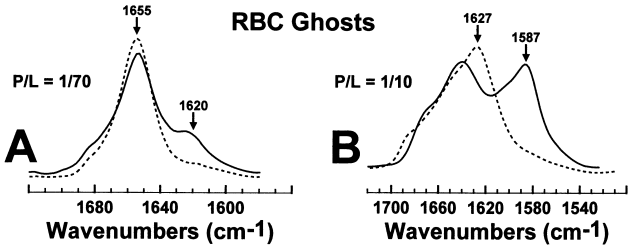

Fig. 13. FTIR spectra of the amide I band for the ^{12}C-carbonyl (i.e. 'native') FP peptide (dashed lines) and the ^{13}C-carbonyl-enhanced FP_{G5-A15} (solid lines) in human RBC (RBC) ghosts, at P/L ratios of 1/70 (A) or 1/10 (B). Using a concentrated peptide–HFIP stock solution, FP was added to ghosts suspended in 5 mM phosphate buffer (pH 7.0) to yield the indicated P/L ratio and a final HFIP concentration of 3%; control ghosts were similarly prepared but omitting peptide. FTIR spectra of peptide in ghosts at 25°C were obtained by subtraction of the control ghost spectrum from the corresponding spectrum of peptide in ghosts with 3% HFIP. (A) FP_{G5-A15} (solid line), FP (dashed line), at a P/L ratio of 1/70. The amide I band is shown for the native FP spectrum, with a dominant α-helical component centered at 1655 cm^{-1}. The new peak at 1620 cm^{-1} in the FP_{G5-A15} spectrum indicates an α-helical component for Gly-5, Ala-6, Leu-7, Phe-8, Leu-9, Gly-10, Phe-11, Leu-12, Gly-13, Ala-14 and Ala-15. (B) FP_{G5-A15} (solid line), FP (dashed line), at a P/L ratio of 1/10. The amide I band is shown for the native FP spectrum, with a major peak at 1627 cm^{-1} and a minor peak at 1688 cm^{-1} indicating a strong β-sheet component. The new major peak at 1587 cm^{-1} in the FP_{G5-A15} spectrum indicates a β-sheet structure for Gly-5, Ala-6, Leu-7, Phe-8, Leu-9, Gly-10, Phe-11, Leu-12, Gly-13, Ala-14 and Ala-15. The abscissas for the A and B spectra (left to right) are 1720–1560 cm^{-1} and 1720–1500 cm^{-1}, respectively, while the ordinates represent absorption (in arbitrary units).

Gly-5 through Ala-15 folding as antiparallel β-sheet at high peptide loading in ghosts [56].

Additional ^{12}C- and ^{13}C-FTIR spectroscopy was performed to investigate both the overall structure and residue-specific conformation of FP in lipid extracts from human erythrocytes. In previous conventional ^{12}C-FTIR experiments on FP with lipid extracts from human red cells [17], a dominant peak at 1656 cm^{-1} was observed at a low P/L ratio of 1/200 indicating high levels of α-helix. At a higher P/L ratio of 1/30, however, the major peak for FP in ghost lipids was shifted to approx. 1634 cm^{-1} and a residual high-field shoulder occurred at 1656 cm^{-1}, consistent with the formation of extensive antiparallel β-sheet coexisting with some α-helix [17]. With a low P/L ratio of 1/70, we find here a principal band occurring at 1656 cm^{-1} for conventional ^{12}C-FTIR

spectra of FP added to lipid extracts from human erythrocyte ghosts (Fig. 14A), in accord with high α-helical content for FP in ghost lipids and in agreement with earlier FTIR studies [17]. A large reduction occurs in the region 1674–1633 cm^{-1} for the FP_{G5-A15} spectrum with a major new peak centered at 1618 cm^{-1} (Fig. 14A), confirming that Gly-5 through Ala-15 assume α-helix conformations in ghost lipids at low loading in a manner similar to that observed for these FP peptides in either HFIP solvent (Fig. 4C) or POPG liposomes (Fig. 8C). The absorption shift caused by incorporation of $^{13}C=O$ for residues Gly-5 through Ala-15 is more dramatic for ghost lipids (Fig. 14A) than ghosts (Fig. 13A), suggesting that FP is a more tightly folded α-helix in ghost lipids than in ghost membranes. At a high P/L ratio of 1/10, the ^{12}C-FTIR spectrum of FP with ghost lipids at (Fig. 14B) showed a dominant peak at 1624 cm^{-1}, and a small high-field peak at 1686 cm^{-1}, reflecting antiparallel β-sheet analogous to that observed earlier [17]. A decrease in absorption occurs in the range 1641–1608 cm^{-1} for the FP_{G5-A15} spectrum with a predominant new peak centered at 1586 cm^{-1} (Fig. 14B), indicating that Gly-5 through Ala-15 fold as antiparallel β-sheet at high peptide loading in ghost lipids. Also of interest are the comparable FTIR spectra of FP and FP_{G5-A15} in either erythrocyte ghosts (Fig. 13B) or lipid extracts (Fig. 14B), suggesting equivalently high levels of antiparallel β-sheet for FP in these systems at high loading.

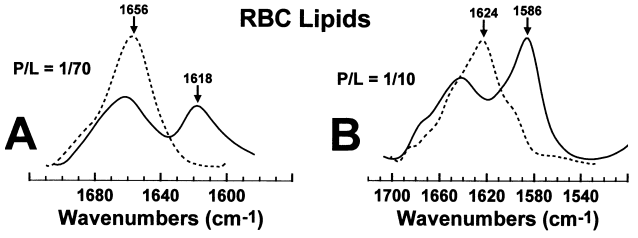

Fig. 14. FTIR spectra of the amide I band for the ^{12}C-carbonyl (i.e. 'native') FP peptide (dashed lines) and the ^{13}C-carbonyl-enhanced FP_{G5-A15} (solid lines) in liposomes prepared from lipid extracts of human RBC (RBC) ghosts, at P/L ratios of 1/70 (A) or 1/10 (B). Peptide–lipid films were prepared by air drying an HFIP solution containing both peptides and RBC ghost lipids onto the ATR crystal to form multilayers. The lipid–peptide sample was then hydrated for 2 h by passing D_2O vapor through ports in the ATR attachment cover plate. (A) FP_{G5-A15} (solid line), FP (dashed line), at a P/L ratio of 1/70. The amide I band is shown for the native FP spectrum, with a dominant α-helical component centered at 1656 cm^{-1}. The new peak at 1618 cm^{-1} in the FP_{G5-A15} spectrum indicates a strong α-helical component for Gly-5, Ala-6, Leu-7, Phe-8, Leu-9, Gly-10, Phe-11, Leu-12, Gly-13, Ala-14 and Ala-15. (B) FP_{G5-A15} (solid line), FP (dashed line), at a P/L ratio of 1/10. The amide I band is shown for the native FP spectrum, with a major peak at 1624 cm^{-1} and a minor peak at 1686 cm^{-1} indicating a strong β-sheet component. The new major peak at 1587 cm^{-1} in the FP_{G5-A15} spectrum indicates β-sheet structure for Gly-5, Ala-6, Leu-7, Phe-8, Leu-9, Gly-10, Phe-11, Leu-12, Gly-13, Ala-14 and Ala-15. The abscissas for the A and B spectra (left to right) are 1720–1560 cm^{-1} and 1720–1500 cm^{-1}, respectively, while the ordinates represent absorption (in arbitrary units).

4. Discussion

The present findings highlight the utility of ^{13}C-enhanced FTIR spectroscopy in studying the conformational flexibility of HIV-1 FP. Earlier Chou–Fasman analysis predicted α-helix for residues 1–18 of FP [17], and high α-helix was confirmed from CD or conventional ^{12}C-FTIR spectra of FP in the HFIP solvent, POPG liposomes (Fig. 2; Table 1), and human erythrocyte ghosts and lipid extracts at low peptide loading (Figs. 13A and 14A). Nevertheless, Chou–Fasman analysis did not successfully predict the higher levels of β- and random structure in this region observed here from CD and FTIR spectra of FP in TFE solution, PBS (Fig. 2; Table 1), or human erythrocyte ghosts and lipid extracts at high peptide loading (Figs. 13B and 14B). The failure of computer algorithms such as Chou–Fasman to predict these structural polymorphisms emphasizes the importance of using residue-specific physical techniques. Moreover, neither CD nor conventional ^{12}C-FTIR spectroscopy can provide mechanistic details on the conformational changes that FP undergoes, as they are global techniques that measure only average FP conformations. In this study, isotope-enhanced ^{13}C-FTIR spectroscopy of FP permitted mapping of the molecular changes accompanying the conversion of α-helix to random and β-structures that occurs with increasing water content. Under conditions of high hydrophobicity, ^{13}C-FTIR spectra of FP peptides in POPG liposomes indicated α-helix for residues 1–16 (Figs. 6, 8 and 10). With the slightly more polar HFIP solvent, both ^{13}C-FTIR spectra (Figs. 4, 6 and 9A–C) and molecular modeling (Fig. 11A,B)

showed that the α-helix was largely conserved, except for a partial fraying of the N-terminal Ala-1 and Val-2 residues. ^{13}C-FTIR spectra demonstrated that the still more polar TFE solvent further converted FP residues 1–7 into β- and random conformations, and even created mixes of α-helix, β- and random structures for the core FP residues 7–16 (Figs. 6, 7 and 9D–F). Using both CD and conventional ^{12}C-FTIR spectroscopy (Fig. 2A; Table 1), FP in PBS buffer was observed to form extensive antiparallel β-sheets with minimal α-helix. Our results demonstrating that the FP conformation is sensitive to environmental polarity are broadly in agreement with earlier 2D-NMR spectroscopic analyses of FP in aqueous, structure-promoting solvents and SDS micelles [48,49].

Conventional ^{12}C-FTIR and ^{13}C-enhanced FTIR spectroscopy were also employed here to assess the conformational changes that occur with increasing FP concentration in erythrocyte ghosts and lipid extracts. With several exceptions [28,35], previous CD or FTIR analyses of synthetic N-terminal gp41 peptides (≤23 residues) with either model [28,39,43,52] or erythrocyte ghost [17] liposomes have identified primarily α-helix at low P/L ratios ($< \sim 1/70$), and β- and random structures at higher P/L ratios ($> \sim 1/50$). Unfortunately, the underlying mechanism for this dose-dependent, conformational change in FP remains unknown, since residue-specific physical measurements were not conducted. In our studies here of either human erythrocyte ghosts or ghost lipid extracts, ^{12}C-FTIR spectra indicate a large α-helical component for FP at low peptide loading (Figs. 13A and 14A). Similar dominant α-helix conformations were detected for FP incorporated into lipids at low loading, from CD or ^{12}C-FTIR spectra of FP with the anionic lipid POPG [28] (Fig. 2D; Table 1), the neutral lipid egg yolk lecithin [52], mixtures of neutral and anionic lipids [43,49] or erythrocyte ghost lipids [17]. The spectral shifts in the ^{13}C-enhanced FTIR spectra of FP_{G5-A15} with either ghosts (Fig. 13A) or lipid extracts (Fig. 14A) at low loading confirm that FP residues Gly-5 to Ala-15 fold as an α-helix, and are similar to that observed with POPG liposomes (Fig. 8C). The high levels of α-helix noted for FP in either ghosts (Fig. 13A) or ghost lipids (Fig. 14A) are consistent with deep penetration of FP into the lipid bilayer at low loading; indeed, FP has been found to bury into the interior of both model lipid bilayers [28,49] and human erythrocyte ghosts [17] at relatively low P/L ratios. It should, however, be pointed out that not all physical studies have determined significant α-helix in model lipids at low FP concentrations. Conventional ^{12}C-FTIR spectra identified predominately β-sheet for FP with either neutral 1-palmitoyl-2-oleoylphosphatidylcholine (POPC) liposomes (P/L ratio ≥ 1/200) [28] or mixed dioleoylphosphatidylcholine/dioleoylphosphatidylethanolamine/cholesterol vesicles (P/L ≥ 1/800) [35]; the disparate findings obtained in these studies and those above indicating substantial α-helix at low FP loading may possibly be due to differences in the choice of lipids and sample preparation. Also of interest is the recent solid-state ^{13}C-enhanced NMR evidence for FP folded as extended β-strand conformation, with peptide bound to lipid mixtures of POPC/POPE/dimyristoyl-*sn*-glycero-3-[phospho-L-serine]/cholesterol for P/L ratios ≥ 1/200 [36]. Unfortunately, NMR measurements were limited to observations at −50°C, and independent experiments using alternative techniques (e.g. CD or FTIR spectroscopy) were not performed to evaluate whether the use of such low temperatures perturbed the overall FP conformation [36].

With erythrocyte ghosts or ghost lipid extracts at higher P/L ratios of 1/10, however, ^{12}C-FTIR spectra showed that FP predominantly assumes an antiparallel β-sheet conformation (Figs. 13B and 14B). Primarily β-sheet was observed for HIV-1 FP in lipids at high loading, from CD or ^{12}C-FTIR spectra of FP with the anionic lipid POPG [28], the neutral lipids POPC [28] and egg yolk lecithin [52], mixtures of neutral and anionic lipids [35,43,53] or erythrocyte ghost lipids [17]. Since previous ESR experiments with spin-labeled FP incorporated into human erythrocyte ghosts indicated peptide clustering at elevated concentrations [17], the ^{12}C-FTIR spectral alterations noted at high loading in either ghosts or ghost lipids (Figs. 13B and 14B) are likely due to membrane-bound FP aggregates. Such membrane-bound FP aggregates are also probably composed of extensive antiparallel β-sheets exposed to water, given the similarities between the ^{12}C-FTIR spectra of high-loaded FP in ghosts and lipid extracts (Figs. 13B and 14B) with that of FP in PBS (Fig. 2A). Membrane-associated FP at high loading might be a

loosely bound, surface-located component, perhaps related to the filamentous, 'amyloid-like' structures observed for N-terminal HIV-1 gp41 peptides in aqueous media [30]. Alternatively, at high peptide loading in either ghosts or lipid extracts, deeply inserted α-helical FP may aggregate to disrupt the lipid bilayer and increase the water content, thereby shifting FP from α-helix to extended β-sheet [53]. With $FP_{G5–A15}$ added to erythrocyte ghosts or lipid extracts at high loading, the ^{13}C-FTIR spectra demonstrated a large shift ($\sim$38 cm^{-1}) from the β-sheet maximum ($\sim$1624–1627 cm^{-1}) in the corresponding ^{12}C-FTIR spectra (Figs. 13B and 14B). These ^{13}C-FTIR spectral findings argue that FP residues Gly-5 to Ala-15 directly participate in the hydrogen-bonded, antiparallel β-sheet, and are in accord with the recent solid-state, ^{13}C-enhanced NMR analysis of FP bound to mixed liposomes indicating that residues Ala-1 to Ala-15 are extended β-strands [36]. Also, it should be noted that the ^{13}C-FTIR spectral shifts for $FP_{G5–A15}$ in erythrocyte ghosts (Fig. 13B) or lipids (Fig. 14B) are very similar to those reported in earlier ^{13}C-FTIR spectra of aqueous amyloid peptides [56–58], supporting the hypothesis that the N-terminal HIV-1 gp41 domain belongs to the prion class of peptides that form β-sheet amyloid fibrils [93,94].

The above ^{13}C-FTIR analysis of FP in POPG liposomes (Figs. 6, 8 and 10) represents a major advance over past residue-specific investigations, because it permits direct measurements on peptide structure in lipid bilayers at physiologically relevant temperatures. For example, most previous residue-specific physical experiments on FP were limited to organic solvents (e.g. TFE or HFIP) [43,48,49,51] or detergent micelles [49], and use of these membrane-mimics may be successful only as a first approximation in simulating FP structure in lipid bilayers. One recent solid-state, ^{13}C-NMR study reported the residue-specific conformation of FP bound to mixed lipid vesicles at −50°C (see above) [36], but it is unclear whether this peptide structure is maintained at physiologic temperatures. Here, we find from ^{13}C-FTIR spectroscopy and molecular modeling of FP in POPG liposomes that residues 1–16 fold as an α-helix, with extended β- and random structures (residues 17–23) having a high degree of flexibility (Figs. 6, 8 and 10). Although earlier residue-specific investigations on FP in membrane-mimics indicate structural models that broadly agree with those obtained from ^{13}C-FTIR spectra of FP in POPG, significant 'fine-structure' discrepancies are nevertheless seen. ^{13}C-FTIR spectra of FP in either HFIP (Figs. 4A, 5A and 6) or TFE (Figs. 6 and 7A,B and 9D), as well as 2D-NMR analysis of FP in SDS or TFE [49], indicated fraying of the α-helix at the N-terminus, which is not observed in ^{13}C-FTIR spectroscopy of FP in POPG liposomes (Fig. 8A). The participation of the N-terminal residues in the α-helix determined here for FP in POPG may be relevant in HIV-cell fusion, since removal of as few as three residues from the N-terminus of gp41 markedly diminished syncytia formation of $CD4^+$ cells transfected with this deletion mutant [25]. On the other hand, a range of physical–biochemical techniques confirmed that residues Gly-13, Ala-14, Ala-15 and Gly-16 participate in the C-terminal cap of the α-helix, regardless of whether FP is incorporated into membrane-mimics or bilayer lipids (Figs. 6 and 11) [48–51]. Based on the ^{13}C-FTIR spectroscopic results and energy minimization results presented here, our model for FP in either the HFIP solvent (Figs. 6 and 11) or POPG liposomes (Fig. 6) indicates that the carboxyl terminus of the helix is a glycine-based cap at Ala-15 known as the α_L motif [95], in which Gly-16 assumes a left-handed conformation and a single hydrogen bond occurs between the $>$N-H at Gly-16 and the $>$C=O at Leu-12. Chang et al. [49] proposed that the residues Ala-15 and Gly-16 lie at the lipid polar head group–water interface, consistent with previous findings of deep penetration of the FP α-helix into the lipid bilayer interior [17]. It is of interest to note that this C-capping sequence (i.e. Gly-13, Ala-14, Ala-15, Gly-16) in the N-terminal gp41 peptide is highly conserved among all known HIV isolates [64]. Given the large genomic divergence among viral isolates [64], this well-conserved, α-helical C-cap may play critical functional roles in HIV processes (e.g. infection, pathogenesis). Last, it is important to note that the detailed α-helical structure determined here for FP in POPG liposomes (Fig. 6) may also occur in host cell plasma membranes, given our ^{13}C-FTIR findings of comparable α-helical structures for FP in RBC ghosts and ghost lipid extracts (Figs. 13A and 14A).

The residue-specific structures determined here for

HIV-1 FP may provide further information on how this gp41 domain participates in viral infection. HIV-1 entry into cells is a two-step process [96], in which the virus binds to cell receptors and then promotes fusion between the opposing lipid bilayers of the viral envelope and cell surface [18,19]. The binding of viral gp120 with cell receptors may expose activated FP [5,97], which may in turn attack the host–cell surface. Although the conformation and location of the FP have not been identified in earlier X-ray diffraction studies of gp41 fragments [10–12,47], this domain may associate with the host–cell surface membrane as a trimer. Since the lipid composition of erythrocyte ghosts is comparable to that of the lymphocyte plasma membrane [18], the residue-specific structures detected here (i.e. α-helix or β-sheet) for FP in ghost membranes (Figs. 13 and 14) may similarly occur in the host–cell surface, serving as an anchor to draw the virus to the target cell [38]. An interesting variation of this 'prefusion' model hypothesizes that the activated fusion peptides simultaneously bind to both viral and target membranes, bringing them into close apposition [2]. That FP could loop back and interact with the HIV-1 envelope by assuming α-helix and/or β-structures as in erythrocyte ghosts and lipid extracts (Figs. 13 and 14) is suggested by the nearly identical lipid compositions reported for erythrocyte ghosts and the HIV envelope [18]. Experimental support for HIV-1 FP joining the viral envelope and targets cells comes from our earlier results showing that synthetic FP is a potent erythrocyte-aggregating agent [38,42,43]. Besides its role in aggregating the viral envelope with host cells, the N-terminal domain of gp41 may also be more directly involved in perturbing membranes critical for HIV-1 infection. As indicated in Section 1, synthetic peptides based on the N-terminal domain of gp41 induce leakage and/or fusion of not only model liposomes [27–35,39–41] but also human erythrocytes and $CD4^+$ lymphocytes [37,42]. Although there is no generally accepted model for how HIV-1 fusion peptides induce their cytolytic and fusogenic activities, earlier work has indicated possible roles for the deep insertion of peptides into lipid bilayers [17,28,35,49], oblique intercalation of α-helical peptide into membrane lipids [31,39,98, 99], membrane aggregation of peptides [17,40, 53], formation of membrane-associated peptide in β-conformations [17,32,33,36,53], peptide induction of non-bilayer lipid [100–102], or creation of peptide-membrane pores [2,53,96]. It is of particular interest that sequence modifications in the N-terminal gp41 domain reduced HIV infectivity and syncytia formation in prior site-directed mutagenesis experiments, and these alterations similarly blunted peptide-induced lysis and fusion with either red cells [42,43] or model liposomes [27,33,35,39,40]. Future application of residue-specific techniques (e.g. ^{13}C-FTIR or ESR spectroscopy of spin-labeled peptides) to these fusion-defective FP variants may indicate whether the detailed conformations determined here, or if any of the above proposed mechanisms of action, for FP play a role in membrane perturbations.

The results obtained here on HIV-1 FP indicate that the joint use of ^{13}C-FTIR spectroscopy and energy minimizations will be of general utility in mapping the secondary structures of peptides and proteins, especially in membrane environments that have been difficult to characterize with X-ray crystallography or 2D-NMR spectroscopy. FTIR analysis of peptides substituted with ^{13}C-labeled carbonyls is a non-perturbing methodology that permits direct assessment of local peptide conformations in membrane-mimics, lipids and membranes. In previous experiments [63], ^{13}C-FTIR spectroscopy has been combined with energy minimizations and molecular simulations to provide an amino acid resolution model of SP-B_{1-25} in POPG lipid, which specified locations for β-sheet, α-helix and random conformations (PDB accession code: 1DFW). In the present work, we find from ^{13}C-FTIR spectroscopy and energy minimizations of FP in HFIP solvent that residues 3–16 fold as an α-helix, with extended β- and random structure residues (1–2 and 17–23) having a high degree of flexibility (PDB accession code: 1ERF) (Figs. 6 and 11A,B). Similar studies indicated a model for FP in POPG (Fig. 6) nearly identical to that for FP in HFIP (Fig. 11A,B), except that residues Ala-1 and Val-2 also participate in the α-helix. We anticipate that analogous residue-specific, ^{13}C-enhanced FTIR spectroscopy and energy minimizations may also elucidate the structures of other lipid bilayer-bound proteins and peptides. Such analyses could greatly assist ongoing structural genomics projects which aim to yield a complete set of protein folds [103], particularly since ~20–30% of the hu-

man genome codes for membrane proteins [104], but few membrane-bound proteins have been structurally determined [103]. Also of interest is our finding that the conformation of the core region of FP may be elucidated in such biological membranes as erythrocytes using heavily ^{13}C-labeled peptides (Figs. 13 and 14). This technique is an extension of previous ^{13}C-FTIR experiments using proteins that were uniformly labeled with ^{13}C-carbonyls (i.e. 'isotope-edited') to examine the secondary structure in both protein–peptide [105] and protein–protein [106] complexes. Our results indicate that this ^{13}C-FTIR methodology may provide unique, residue-specific information on other protein and peptide conformations in biomembranes.

Acknowledgements

We thank the reviewers for helpful comments, and Dr. James Bowie (UCLA) for advice and use of the AVIV 62DS spectropolarimeter. The Beckman Research Institute of the City of Hope core facility was supported by Cancer Center Support Grant P30 CA33572. This study was supported by NIH MBRS Grants GM 08140 (L.M.G., A.J.W.) and GM 53933-03 (P.W.M.), and a California State University Program for Education and Research in Biotechnology (CSUPERB) Grant (P.W.M.). The ABI 431A peptide synthesizer was obtained with NIH Small Equipment Grant GM 50483 (L.M.G., A.J.W.), the Protein Technologies Symphony/Multiplex SPPS synthesizer was acquired with a NIH National Center for Research Resources Shared Instrumentation Grant 1 S10 RR14867-01A1 (M.R. Yeaman, A.J.W.) and the REI Bruker Vector 22 FTIR spectrometer was funded by a grant from the Harbor-UCLA REI Common Use and Replacement Equipment Program (A.J.W.). FTIR spectral data acquisition and analysis were supported by the Drew University RCMI Bioinformatics Core Grant (NCRR/RCMI G12 RR 03026).

References

[1] J.M. McCune, L.B. Rabin, M.B. Feinberg, M. Lieberman, J.C. Kosek, G.R. Reyes, I.L. Weisman, Cell 53 (1988) 55–67.
[2] J. White, Science 258 (1992) 917–924.
[3] W.R. Gallaher, Cell 50 (1987) 327–328.
[4] F. Gonzalez-Scarano, M.N. Waxham, A.M. Ross, J.A. Hoxie, AIDS Res. Hum. Retroviruses 3 (1987) 245–252.
[5] T.K. Hart, A. Truneh, P.J. Bugelski, AIDS Res. Hum. Retroviruses 12 (1996) 1305–1313.
[6] M. Lu, S.C. Blacklow, P.S. Kim, Nat. Struct. Biol. 2 (1995) 1075–1082.
[7] M. Rabenstein, Y.-K. Shin, Biochemistry 34 (1995) 13390–13397.
[8] M.D. Rabenstein, Y.-K. Shin, Biochemistry 35 (1996) 13922–13928.
[9] M. Lu, P.S. Kim, J. Biomol. Struct. Dyn. 15 (1997) 465–471.
[10] D.C. Chan, D. Fass, M. Berger, P.S. Kim, Cell 89 (1997) 263–273.
[11] W. Weissenhorn, A. Dessen, S.C. Harrison, J.J. Skehel, D.C. Wiley, Nature 387 (1997) 426–430.
[12] P.T. Wingfield, S.J. Stahl, J. Kaufman, A. Zlotnick, C.G. Hyde, A.M. Gronenborn, G.M. Clore, Protein Sci. 6 (1997) 1653–1660.
[13] M. Caffrey, J. Kaufman, S. Stahl, P.T. Wingfield, A.M. Gronenborn, G.M. Clore, Protein Sci. 8 (1999) 1904–1907.
[14] D.-K. Chang, S.-F. Cheng, V.D. Trivedi, J. Biol. Chem. 274 (1999) 5299–5309.
[15] P.A. Bullough, F.M. Hughson, J.J. Skehel, D.C. Wiley, Nature 371 (1994) 37–43.
[16] C.M. Carr, P.S. Kim, Cell 73 (1993) 823–832.
[17] L.M. Gordon, C.C. Curtain, Y.C. Zhong, A. Kirkpatrick, P.W. Mobley, A.J. Waring, Biochim. Biophys. Acta 1139 (1992) 257–274.
[18] R.C. Aloia, F.C. Jensen, C.C. Curtain, P.W. Mobley, L.M. Gordon, Proc. Natl. Acad. Sci. USA 85 (1988) 900–904.
[19] L.M. Gordon, F.C. Jensen, C.C. Curtain, P.W. Mobley, R.C. Aloia, Biochim. Biophys. Acta 943 (1988) 331–342.
[20] J. Felser, T. Klimkait, J. Silver, Virology 170 (1989) 566–570.
[21] E.O. Freed, D.J. Myers, R. Risser, Proc. Natl. Acad. Sci. USA 87 (1990) 4650–4654.
[22] E.O. Freed, E.L. Delwart, G.L. Buchschacher Jr., A.T. Panganiban, Proc. Natl. Acad. Sci. USA 89 (1992) 70–74.
[23] L. Bergeron, N. Sullivan, J. Sodroski, J. Virol. 66 (1992) 2389–2397.
[24] K. Salzwedel, E.A. Berger, Proc. Natl. Acad. Sci. USA 97 (2000) 12794–12799.
[25] H. Schaal, M. Klein, P. Gehrmann, O. Adams, A. Scheid, J. Virol. 69 (1995) 3308–3314.
[26] M.D. Delahunty, I. Rhee, E.O. Freed, J.S. Bonifacino, Virology 218 (1996) 94–102.
[27] M. Pritsker, J. Rucker, T.L. Hoffman, R.W. Doms, Y. Shai, Biochemistry 38 (1999) 11359–11371.
[28] M. Rafalski, J.D. Lear, W.F. DeGrado, Biochemistry 29 (1990) 7917–7922.
[29] V.A. Slepushkin, G.B. Melikyan, M.V. Sidorova, V.M. Chumakov, S.M. Andreev, R.A. Manukyan, E.V. Karamov, Biochem. Biophys. Res. Commun. 172 (1990) 952–957.
[30] V.A. Slepushkin, S.M. Andreev, M.V. Sidorova, G.B. Me-

likyan, V.B. Grigoriev, V.M. Chumakov, A.E. Grinfeldt, R.A. Manukyan, E.V. Karamov, AIDS Res. Hum. Retroviruses 8 (1992) 9–18.
[31] I. Martin, F. Defrise-Quertain, E. Decroly, M. Vandenbranden, R. Brasseur, J.-M. Ruysschaert, Biochim. Biophys. Acta 1145 (1993) 124–133.
[32] J.L. Nieva, S. Nir, A. Muga, F.M. Goni, J. Wilschut, Biochemistry 33 (1994) 3201–3209.
[33] F.B. Pereira, F.M. Goni, J.L. Nieva, FEBS Lett. 362 (1995) 243–246.
[34] Y.T. Terletskaya, I.O. Trikash, E.S. Serdyuk, S.M. Andreev, Biochemistry (Moscow) 60 (1995) 1309–1314.
[35] F.B. Pereira, F.M. Goni, J.L. Nieva, Biophys. J. 73 (1997) 1977–1986.
[36] J. Yang, C.M. Gabrys, D.P. Weliky, Biochemistry 40 (2001) 8126–8137.
[37] P.W. Mobley, C.C. Curtain, A. Kirkpatrick, M. Rostamkhani, A.J. Waring, L.M. Gordon, Biochim. Biophys. Acta 1139 (1992) 251–256.
[38] P.W. Mobley, R. Pilpa, C. Brown, A.J. Waring, L.M. Gordon, AIDS Res. Hum. Retroviruses 17 (2001) 311–327.
[39] I. Martin, H. Schaal, A. Scheid, J.-M. Ruysschaert, J. Virol. 70 (1996) 298–304.
[40] Y. Kliger, A. Aharoni, D. Rapaport, P. Jones, R. Blumenthal, Y. Shai, J. Biol. Chem. 272 (1997) 13496–13505.
[41] S.G. Peisajovich, R.F. Epand, M. Pritsker, Y. Shai, R.M. Epand, Biochemistry 39 (2000) 1826–1833.
[42] P.W. Mobley, H.-F. Lee, C.C. Curtain, A. Kirkpatrick, A.J. Waring, L.M. Gordon, Biochim. Biophys. Acta 1271 (1995) 304–315.
[43] P.W. Mobley, A.J. Waring, M.A. Sherman, L.M. Gordon, Biochim. Biophys. Acta 1418 (1999) 1–18.
[44] S. Jiang, K. Lin, N. Strick, A.R. Neurath, Biochem. Biophys. Res. Commun. 195 (1993) 533–538.
[45] L.M. Gordon, A.J. Waring, C.C. Curtain, A. Kirkpatrick, C. Leung, K. Faull, P.W. Mobley, AIDS Res. Hum. Retroviruses 11 (1995) 677–686.
[46] F.B. Pereira, F.M. Goni, J.L. Nieva, AIDS Res. Hum. Retroviruses 13 (1997) 1203–1211.
[47] K. Tan, J.-H. Liu, J.-H. Wang, S. Shen, M. Lu, Proc. Natl. Acad. Sci. USA 94 (1997) 12303–12308.
[48] D.-K. Chang, W.-J. Chien, S.-F. Cheng, Eur. J. Biochem. 247 (1997) 896–905.
[49] D.-K. Chang, S.-F. Cheng, W.-J. Chien, J. Virol. 71 (1997) 6593–6602.
[50] P. Vidal, L. Chaloin, A. Heitz, N. Van Mau, J. Mery, G. Divita, F. Heitz, J. Membr. Biol. 162 (1998) 259–264.
[51] A.J. Waring, P.W. Mobley, L.M. Gordon, Proteins Struct. Funct. Genet. Suppl. 2 (1998) 38–49.
[52] C.C. Curtain, F. Separovic, K. Nielsen, D. Craik, Y.C. Zhong, A. Kirkpatrick, Eur. Biophys. J. 28 (1999) 427–436.
[53] G. Schwarz, S.E. Taylor, Biophys. J. 76 (1999) 3167–3175.
[54] L. Tadesse, R. Nazarbaghi, L. Walters, J. Am. Chem. Soc. 113 (1991) 7036–7037.
[55] S.M. Decatur, Biopolymers 54 (2000) 180–185.
[56] K.J. Halverson, I. Sucholeiki, T.T. Ashburn, P.T. Lansbury Jr., J. Am. Chem. Soc. 113 (1991) 6701–6703.
[57] T.T. Ashburn, M. Auger, P.T. Lansbury Jr., J. Am. Chem. Soc. 114 (1992) 790–791.
[58] M.A. Baldwin, Methods Enzymol. 309 (1999) 576–591.
[59] E.S. Manas, Z. Getahun, W.W. Wright, W.F. DeGrado, J.M. Vanderokooi, J. Am. Chem. Soc. 122 (2000) 9883–9890.
[60] C.F.C. Ludlam, I.T. Arkin, X.-M. Liu, M.S. Rothman, P. Rath, S. Aimoto, S.O. Smith, D.M. Engelman, K.J. Rothschild, Biophys. J. 70 (1996) 1728–1736.
[61] A. Kukol, I.T. Arkin, Biophys. J. 77 (2000) 1594–1601.
[62] S.A. Tatulian, L.K. Tamm, Biochemistry 39 (2000) 496–507.
[63] L.M. Gordon, K.Y.C. Lee, J.A. Zasadzinski, F.J. Walther, M.A. Sherman, A.J. Waring, J. Pept. Res. 55 (2000) 330–347.
[64] G. Myers, B. Korber, J.A. Berzofsky, R.F. Smith, G.N. Pavalakis, in: Human Retroviruses and AIDS 1991: a Compilation and Analysis of Nucleic Acid and Amino Acid Sequences, Los Alamos National Lab., Los Alamos, NM, 1991, pp. 11–81.
[65] D. Eisenberg, M. Wesson, Biopolymers 29 (1990) 171–177.
[66] A.J. Waring, S.S.L. Harwig, R.I. Lehrer, Protein Pept. Lett. 3 (1996) 177–184.
[67] M.L. Longo, A.J. Waring, L.M. Gordon, D.A. Hammer, Langmuir 14 (1998) 2385–2395.
[68] J.T. Dodge, C. Mitchell, D.J. Hanahan, Arch. Biochem. Biophys. 100 (1963) 119–130.
[69] E. Peuchant, R. Wolff, C. Salles, R. Jensen, Anal. Biochem. 181 (1989) 341–344.
[70] L.M. Gordon, S. Horvath, M.L. Longo, J.A. Zasadzinski, W. Taeusch, K. Faull, C. Leung, A.J. Waring, Protein Sci. 5 (1996) 1662–1675.
[71] A.J. Waring, K.F. Faull, C. Leung, A. Chang-Chien, P. Mercado, H.W. Taeusch, L.M. Gordon, Pept. Res. 9 (1996) 28–39.
[72] W.C.J. Johnson, Proteins Struct. Funct. Genet. 7 (1990) 205–214.
[73] Y.H. Chen, J.T. Yang, K.H. Chau, Biochemistry 13 (1974) 3350–3359.
[74] J. Kauppine, D. Moffatt, H.H. Mantsch, D. Cameron, Appl. Spectr. 35 (1981) 272–278.
[75] D.M. Byler, H. Susi, Biopolymers 25 (1986) 469–487.
[76] W.K. Surewicz, H.H. Mantsch, Biochim. Biophys. Acta 952 (1988) 115–130.
[77] E. Goormaghtigh, V. Raussens, J.-M. Ruysschaert, Biochim. Biophys. Acta 1422 (1999) 105–185.
[78] C.M. Deber, Macromolecules 7 (1974) 47–51.
[79] A.M. Dwivedi, S. Krimm, Biopolymers 23 (1984) 923–943.
[80] P.I. Haris, D. Chapman, Biochemistry 31 (1992) 6279–6284.
[81] S. Krimm, J. Bandekar, Adv. Protein Chem. 38 (1986) 181–364.
[82] W.H. Moore, S. Krimm, Biopolymers 15 (1976) 2439–2464.
[83] W.H. Moore, S. Krimm, Biopolymers 15 (1976) 2465–2483.
[84] P. Dauber-Osguthorpe, V.A. Robert, D.J. Osguthorpe,

J. Wolff, M. Genest, A.T. Hagler, Proteins Struct. Funct. Genet. 4 (1988) 31–47.
[85] J.R. Maple, U. Dinur, A.T. Hagler, Proc. Natl. Acad. Sci. USA 85 (1988) 5350–5354.
[86] R.A. Laskowski, M. MacArthur, D.S. Moss, J.M. Thornton, J. Appl. Crystallogr. 26 (1993) 283–291.
[87] L.G.J. Hammarstrom, T.J. Gauthier, R.P. Hammer, M.L. McLaughlin, J. Pept. Res. 58 (2001) 108–116.
[88] L.M. Gordon, C.C. Curtain, V. McCloyn, A. Kirkpatrick, P.W. Mobley, A.J. Waring, AIDS Res. Hum. Retroviruses 9 (1993) 1145–1156.
[89] P.I. Haris, D. Chapman, Biopolymers 37 (1995) 251–263.
[90] S.J. Prestrelski, D.M. Byler, M.P. Thompson, Int. J. Pept. Protein Res. 37 (1991) 508–512.
[91] H. Susi, D.M. Byler, Biochem. Biophys. Res. Commun. 115 (1983) 391–397.
[92] Y. Gong, H.X. Zhou, M. Guo, N.R. Kallenbach, Protein Sci. 4 (1995) 1446–1456.
[93] I. Callebaut, A. Tasso, R. Brasseur, A. Burny, D. Portetelle, J.P. Mornon, J. Comput.-Aided Mol. Des. 8 (1994) 175–191.
[94] J.L. Nieva, F.M. Goni, A.L. Mason, A.R. Mock, A. Muga, A. Saez, W.R. Gallaher, Biophys. J. 78 (2000) 412A.
[95] R. Aurora, R. Srinivasan, G.D. Rose, Science 264 (1994) 1126–1130.
[96] E.O. Freed, M.A. Martin, J. Biol. Chem. 270 (1995) 23883–23886.
[97] Q.J. Sattentau, J.P. Moore, J. Exp. Med. 174 (1991) 407–415.
[98] R. Brasseur, B. Cornet, A. Burny, M. Vandenbranden, J.-M. Ruysschaert, AIDS Res. Hum. Retroviruses 4 (1988) 83–90.
[99] J.P. Bradshaw, M.J.M. Darkes, T.A. Harroun, J. Katsaras, R.M. Epand, Biochemistry 39 (2000) 6581–6585.
[100] P.L. Yeagle, R.M. Epand, C.D. Richardson, T.D. Flanagan, Biochim. Biophys. Acta 1065 (1991) 49–53.
[101] R.M. Epand, J.J. Cheetham, R.F. Epand, P.L. Yeagle, C.D. Richardson, Biopolymers 32 (1992) 309–314.
[102] R.F. Epand, I. Martin, J.-M. Ruysschaert, R.M. Epand, Biochem. Biophys. Res. Commun. 205 (1994) 1938–1943.
[103] S.E. Brenner, M. Levitt, Protein Sci. 9 (2000) 197–200.
[104] E. Wallin, G. von Heijne, Protein Sci. 7 (1998) 1029–1038.
[105] M. Zhang, H. Fabian, H.H. Mantsch, H.J. Vogel, Biochemistry 33 (1994) 10883–10888.
[106] K.P. Das, L.-P. Choo-Smith, J.M. Petrash, W.K. Surewicz, J. Biol. Chem. 274 (1999) 33209–33212.